Dust Grain Charging In Tokamak Plasmas

Christopher. M. Bray

Department of Physics, Imperial College London

Submitted in partial fulfilment of the requirements for the degree of Master of Science of Imperial College London

September 2014

I am forever indebted to Imperial College's disability service who have not only provided me with a tutor to help plan this project but also for funding the psychometric assessment which has empowered me to take ownership of my learning difficulty and find ways to overcome it to the best of my ability. The submission of this project symbolises the first step on the path to success and fulfilment.

Declaration

This dissertation amounts to a detailed literature review on topics related to the charging of dust grains in Tokamak plasmas. As such it contains no original Physics. However, I hereby declare that the concept of the work is my own and that every effort has been made to ensure the originality of the written English contained therein. In addition, all of the numerical work and all of the diagrams/graphs are the work of the author unless otherwise stated.

Christopher. M. Bray
September 2014

Acknowledgements

Sincere thanks are due to my supervisor Dr. Michael Coppins and study mentor Ms. Katherine Carpani, who have provided valuable help and incomparable expertise during this short project.

Abstract

The presence of solid, micro-impurtities in tokamak plasmas has become a topic of great importance. Dust, originating from the reactor wall surfaces as a result plasma surface interactions, has the potential to cause serious safety hazards and confinement issues and therefore the transport of these particle contaminants in the plasma of an operational tokamak is therefore, a matter of great importance. An important aspect of Dust transport models is the charge acquired by a dust grain immersed in plasma. This study analyses methods at computing the corresponding 'floating potential'. The orbital motion limited (OML) theory is presented in 4 guises as a means for calculating this floating potential in a tokamak plasma. In addition OML is compared to the ABR model, which assumes that the incoming ion motion is radial. It is found that ABR gives a floating potential that is an explicitly function of dust grain radius in contrast to OML which gives the floating potential as a function of the ration of the ion to electron temperature only. Analysis of the plasma dust interaction suggests that, whilst small dust grains possess more or less the vacuum potential, large grains modify the plasma on scales of λ_D and far beyond to such an extent that the potential structure is very different, and includes potential barriers to ion collection. OML is modified to account for 4 situations, small grain flowless (OML), large grain flowless (MOML), small grain flow (SOML)and large grain flow (SMOML). It is shown that in the context of the dust transport code DTOCKS, in the regime of interest both flow and grain size should be accounted for, and instead of using basic OML, SOML and SMOML should be considered for the charging model.

Table of contents

List of figures

List of tables

Chapter 1

Introduction

1.1 Background and Motivation: Nuclear Fusion

Of all the low carbon methods of energy generation, controlled nuclear fusion, if it proves practical on a industrial scale, is undoubtedly the most attractive. There is good reason to be optimistic, for nuclear fusion could offer electricity generation accompanied by zero Carbon emissions, inherent safety, only small quantities of short half-life nuclear waste and perhaps most importantly, a practically unlimited fuel supply [31]. Nuclear fusion is the fusing of two small nuclei to form a larger one with an accompanying release of energy arising from the conversion of mass to binding energy. In order to achieve fusion a critical triple product of density, temperature and pressure must be satisfied. There are three confinement approaches to maximise this product, namely gravitational confinement (stars), inertial confinement and magnetic confinement [38]. There are many reaction pathways which are energetically favourable. These may be identified using figure 1.1 - any reaction pathway which leads to an increase in binding energy will release energy in the ideal case. Considering Nuclear Fusion for terrestrial energy generation, only the most energetically favourable pathways are useful. By a quirk of nuclear shell structure, the said reactions are just those which result from the fusion of hydrogen isotopes to form Helium-4. Of these reactions the one with the best combination of cross section and net energy release is the Deuterium-Tritium (D-T) pathway, equation 1.1, which releases 17.6MeV per reaction [38].

$$D_1^2 + T_1^3 \rightarrow He_2^4 + n^1 + 17.6MeV \tag{1.1}$$

Despite the energetic advantages of the D-T pathway it has two major drawbacks. Firstly, although Deuterium is relatively abundant, being present with a concentration of 156ppm in naturally occurring Hydrogen, Tritium is scarce and must be bred using Lithium (equa-

tion 1.2). This process is fraught with safety concerns due to the toxicity of Lithium. In addition however, tritium itself is radioactive and highly toxic [10].

$$Li^6 + n \rightarrow He^4 + T + 4.8MeV \tag{1.2}$$

The most promising nuclear fusion device is the 'Tokamak', a magnetic confinement device. In Tokamak conditions, the fuel must be heated to around $100 \times 10^6 K$ and on this temperature scale, the fuel exists in the plasma state. The plasma is so hot that any solid material coming into contact with it would be instantly vaporised and so the plasma must be contained by magnetic fields. Considering the Fusion reaction only, the Tokamak is an inherently safe device since at any one time, only a few grams of fuel is present in the reactor so there is no chance of a runaway reaction. This also means the reactor could be shut down very rapidly unlike a fission plant. Such safety claims are widely proliferated by Tokamak researchers. However, this picture is complicated by the presence of 'dust'.

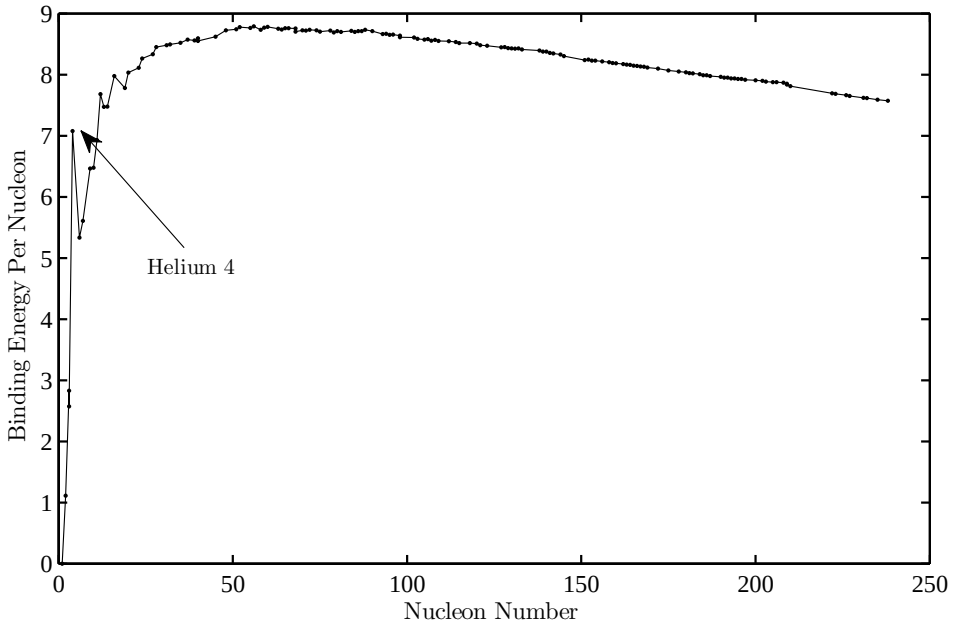

Fig. 1.1 Binding energy vs nucleon number, indicating potential viable fusion reactions for energy generation

1.2 Dust in Fusion Devices

In essence a Tokamak consists of a Torus shaped reactor vessel and an iron core, figure 1.2. The plasma within the reactor vessel acts just like a secondary winding on an ordinary transformer, and the configuration allows large currents to be induced in the plasma. The plasma is subsequently heated by the ohmic effect. Further heating is achieved by the injection of neutral particles (NBI), and/or by radio waves. Together, these methods can take the temeprature of the core plasma up to around $150 \times 10_6 K$ [38], [36] The plasma is confined

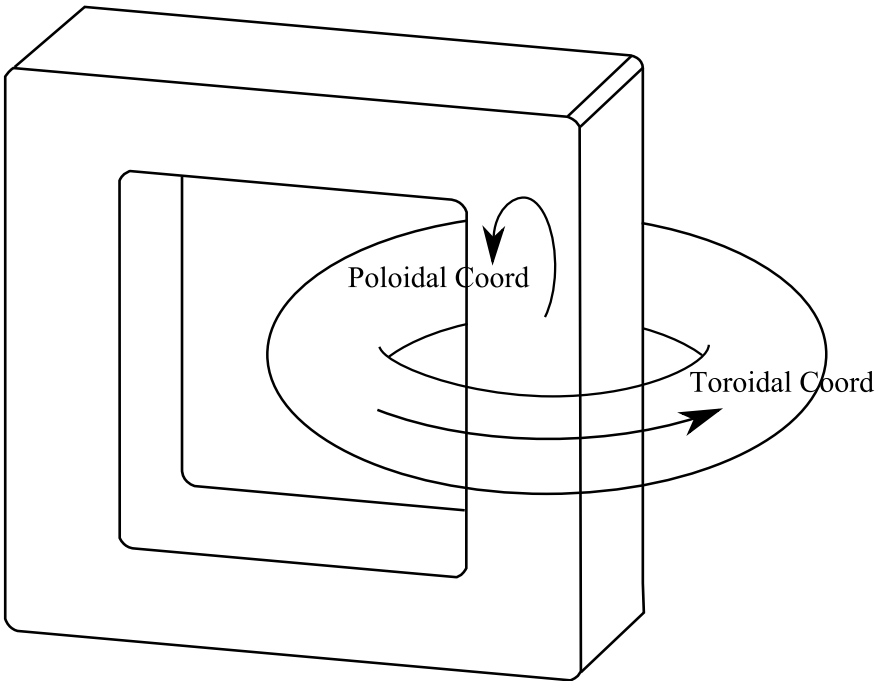

Fig. 1.2 Schematic of Tokamak Geometry Illustrating The Poloidal and Toroidal Directions

within the vessel by a helical magnetic field consisting of nested flux surfaces upon which particles are transported freely but across which transport is strongly suppressed. The helical confinement field is produced by a superposition between the plasma's own poloidal magnetic field and a toroidal magnetic field, generated via external current coils. The boundary between the closed field lines that make up the nested flux surfaces and the open field lines, which end on material targets in the vessel, is called the seperatrix in Divertor Tokamaks. The Divertor consists of a magnetic field configuration along with material targets, Divertor plates, which prevent the hot plasma from coming into contact with the first wall of the reactor vessel, thereby maximising rector life [36]. The region of open field lines is known as the scrape off layer, and it is here that so called 'dust' particles are found. The scrape off layer is at a much lower temperature than the core, and any dust grains transported to the

core are immediately vaporised (reference). The magnetic field configuration is illustrated by the schematic poloidal cross section through a reactor vessel in figureẽffig:pol. Due to

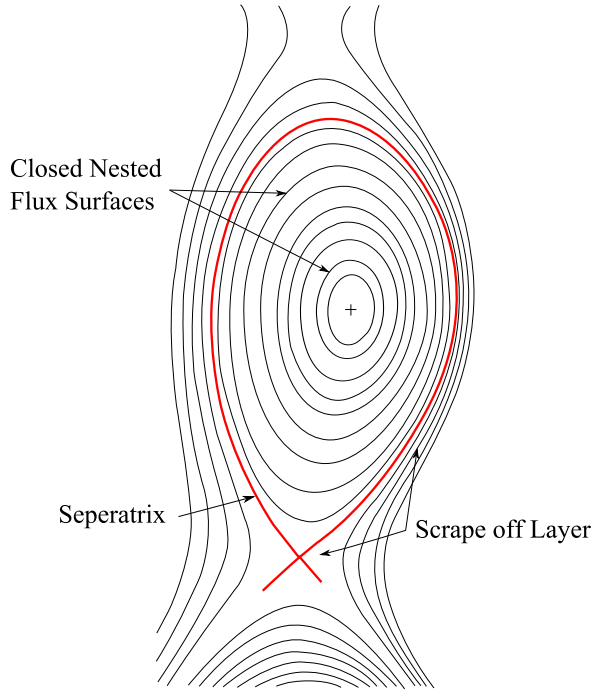

Fig. 1.3 Schematic of a poloidal cross section through a Tokamak showing the nested poloidal flux surfaces, the scrape off layer (SOL), the plasma edge and the last closed flux surface.

the enormous heat loads divertor targets are subject to, they emit impurities via sputtering mechanisms. Despite the divertor targets baring the brunt of the heat load, plasma interactions with the reactor vessel's first wall are unnavoidable leading to more impurities. These solid impurities are called 'dust' and are found in the SOL. ITER's divertors are slated to be of Beryllium (Be) with the first wall of Tungsten (W), so that dust from these elements is expected to be present. Significant safety and operational concerns arise with the presence of dust. Briefly, dust can be either transported to the core, in which case it is vaporised and disrupts fusion whilst also causing significant energy losses due to Bremsstrahlung radiation, or it can be re-deposited on the reactor walls. In the latter case, Tritium absorption by dust grains is a serious safety concern [5]. In order to ensure adequate safety precautions are made against dust, it is vital that engineers can predict where dust will proliferate. To achieve this, physicists must develop accurate dust transport codes. A dust grain immersed in a plasma will naturally acquire a negative charge in the first instance due to collection of electrons on its surface (see Chapter 2). Positive charges are possible too (see Subsection 2.1.1 and Chapter 3). The dust grain charge is a vital component of any Dust transport

code, and there are a variety of theoretical approaches for computing it. Dusty plasma literature will be reviewed in this regard, and predictions for the dust grain charge in a typical steady state Tokamak plasma shall be produced. Before beginning the discussion on charging mechanisms, a brief review of some pre-requisite plasma physics is presented. This dissertation deals with dust grains but it is noted that liquid 'grains' are likely to be significant in number. Plasmas with liquid grains are termed 'misty plasmas' (insert reference).

1.3 Essential Plasma Physics - A Brief Overview

A plasma is a fully ionised gas. As a result the dominant particle-particle interaction is via the Lorentz force and so plasmas exhibit collective behaviour. The number density in the SOL is of the order $10^{18}m^{-3}$, and so an exact solution to this plasma equation of motion requires the solution of 10^{18} coupled differential equations; clearly and intractable problem [36]. Instead, kinetic theory is applied by introducing a distribution function, $f(\vec{r},\vec{v},t)$, defined in a 6 dimensional phase space, whose element $d^3x d^3y d^3z d^3v_x d^3v_y d^3v_z$ shall be denoted $d^3\vec{r}d^3\vec{v}$. The quantity $f(\vec{r},\vec{v},t)d^3\vec{r}d^3\vec{v}$ is defined to be the number of particles in the volume $(x+dx, y+dy, z+dz)$ in configuration space with velocity between $(v_x+dv_x, v_y+dv_y, v_z+dv_z)$. Therefore, defining $n(\vec{r},t)$ and N, the number density distribution function and the total number of particles in the system respectively, we can normalise by distribution function to obtain:

$$n(\vec{r},t) = \int_{-\infty}^{\infty} d\vec{v} f(\vec{r},\vec{v},t) \quad N = \int_{-\infty}^{\infty}\int_{-\infty}^{\infty} d\vec{r}d\vec{v} f(\vec{r},\vec{v},t) \tag{1.3}$$

In a collisionless plasma, such as that existing in a Tokamak, the evolution of the distribution function is governed by the collisionless Vlasov equation 1.4. The connection between observables and the distribution function is found by taking velocity moments of the distribution function. In this way, average plasma quantities are obtained. For instance, the first velocity moment gives the average velocity, $\langle v(\vec{r},t)\rangle$ [38] [1] [34].

$$\frac{\partial f\left(\vec{r},\vec{v},\vec{t}\right)}{\partial t} + \vec{v}\cdot\nabla_r f\left(\vec{r},\vec{v},\vec{t}\right) + \frac{q}{m}\left(\vec{E}+\vec{v}\times\vec{B}\right)\cdot\nabla_v f\left(\vec{r},\vec{v},\vec{t}\right) = 0 \tag{1.4}$$

$$\frac{1}{n(\vec{r},t)}\langle v(\vec{r},t)\rangle = \int_{-\infty}^{\infty} d\vec{v}\vec{v} f(\vec{r},\vec{v},t) \tag{1.5}$$

[1] The plasma pressure, a tensor quantity, obtained by taking the 2nd velocity moment, shall not be required in this review

1.3.1 The Maxwell Boltzmann Distribution (Maxwellian)

The Maxwell Boltzmann distribution, $f_m\left(\vec{v}_j\right)$ written for species j, is valid for collisional plasmas in thermal equilibrium and is given by equation 1.6. The collisions are binary coulomb collisions governed by the Fokker Plank equation, whose only steady state solutions are Maxwellians. This does not mean that evolving plasmas will always or are even likely to have Maxwellian distributions [41]. However, in an approximately steady situation, a Maxwellian distribution is well justified. Despite the fact that Tokamak plasmas are considered to be collisionless, it is generally assumed that the distribution function of thermal ions and electrons in Tokamak plasmas is, to lowest order, Maxwellian [28]. A more detailed discussion on non-Maxwellian distribution functions in Tokamak plasmas is beyond the scope of this short review, but the ubiquity of the assumption in the literature is the main justification for its inclusion here. This is certainly a debatable conclusion.

$$f_m\left(\vec{v}_j\right) = n\left(\frac{\beta}{\pi}\right)^{\frac{3}{2}} \exp\left(-\beta|\vec{v_j}|^2\right) \tag{1.6}$$

Where:

$$\beta = \frac{m}{2k_BT} \tag{1.7}$$

From 1.5 and 1.6, the average velocity of a particle in the Maxwellian plasma is:

$$\langle\vec{v}_j\rangle = \int_{-\infty}^{\infty}\int_{-\infty}^{\infty}\int_{-\infty}^{\infty} dv_x dv_y dv_z \left(\frac{\beta}{\pi}\right)^{\frac{3}{2}} \exp\left(-\beta|\vec{v_j}|^2\right) \tag{1.8}$$

Noting that equation 1.8 is spherically symmetric the average speed may be computed by converting to spherical coordinates with $dv_x dv_y dv_z = v^2 \sin\theta dr d\theta d\phi$, and integrating over all angles to obtain 1.9:

$$\langle v_j\rangle = \left(\frac{8k_BT}{m\pi}\right)^{\frac{1}{2}} \tag{1.9}$$

The particle flux is defined $\vec{\Gamma}_j := n_j\vec{v}_j$. A very useful quantity for dust grain charging (see Chapter 2) is the average one way flux to a surface S immersed in the plasma, $\Gamma_{S,j} = n\langle v_{S,j}\rangle$. The one way flux is useful because the net flux on any symmetrical surface is zero by symmetry. Consider a surface S with unit normal $\hat{S}$. The component of velocity normal to the surface is simply $|\vec{v}||\vec{S}|\cos\theta$. Then $\Gamma_{S,j}$ simplifies to 1.11

$$\Gamma_{s,j} = \frac{n}{\sqrt{\pi}}\beta^{\frac{3}{2}} \int_0^{\frac{\pi}{2}}\int_0^{2\pi}\int_0^{\infty} d\theta d\phi dr \exp(-\beta v_i^2) \tag{1.10}$$

$$\Gamma_s = \frac{n}{4}\langle v_j \rangle \tag{1.11}$$

Again using spherical polars and integrating the Maxwellian over all angles, the Maxwell speed distribution is obtained.

$$f_m(v_j) = 4\pi n \left(\frac{\beta}{\pi}\right)^{\frac{3}{2}} v^2 \exp(-\beta v_j^2) \tag{1.12}$$

In chapter 2, Poisson's equation 1.13 is solved (see 2.2.1), where ϕ is the potential, e is the charge on a singly charged ion, and n_i and n_e are the number densities of the electrons and ions respectively. Solving equation 1.13 requires knowledge of the density distribution function $n(\vec{r},\vec{v},t)$. In the case of a Maxwellian plasma, $n(\vec{r},\vec{v},t)$ can be estimated from the Vlasov equation, which modifies $f_m(v)$ in the presence of an EM field. Considering a spherically symmetric potential with $\vec{B} = 0$, the Vlasov equation becomes 1.14.

$$\nabla^2\phi = \frac{e}{\varepsilon_0}(n_i - n_e) \tag{1.13}$$

$$v_j \frac{\partial}{\partial r}\left[n_j\left(\frac{\beta}{\pi}^{\frac{3}{2}} \exp\left(-\beta v_j^2\right)\right)\right] = \frac{q_j}{m_j}\frac{\partial\phi}{\partial r}\frac{\partial}{\partial v_j}\left[n_j\left(\frac{\beta}{\pi}^{\frac{3}{2}} \exp\left(-\beta v_j^2\right)\right)\right] \tag{1.14}$$

Defining n_∞ as the density given by equation 1.3 and $\phi_\infty = 0$ as the potential at infinity. Integration of equation 1.14 results in the Boltzmann relation, equation 1.15, an approximation widely used in plasma physics [38].

$$n_j = n_\infty \exp\left(\frac{q_j\phi}{k_B T_j}\right) \tag{1.15}$$

It is essential to be precise about its applicability. Strictly speaking of course, with $\vec{B} = 0$, it is invalid everywhere in a Tokamak plasma since magnetic fields on the order of 10^0 to 10^1 are present everywhere [36]. However, on closer inspection it can be argued that under certain circumstances the approximation is, although slightly tenuous, at least defensible. For instance, consider the flow of electrons onto a negatively charged plate immersed in a plasma. If we assume that the system is in equilibrium, the electrons will have a Maxwellian distribution from [28]. Since the electrons are in a repulsive potential, only those electrons on the right tail of the Maxwellian distribution will reach the plate and so the flow of electrons onto the plate will be much slower than the random thermal velocity. In this case, providing the electrostatic potential is adequate, this term will dominate the magnetic term

in the Vlasov equation and then the approximation of $\vec{B} = 0$ is . Of course this argument cannot hold for the ions which find themselves in an attractive potential. In that case the flow towards the surface will be large and the magnetic term can no longer be ignored [36]. Equation 1.6 is only applicable to a stationary plasma whereas a Tokamak plasma possesses large poloidal and toroidal flows. Therefore equation 1.16, the drifting Maxwellian, where v_d is the plasma fluid velocity, shall be useful in charging models which include flow (see 2.2.5 and 2.2.6).

$$f_m(\vec{v}_j) = n_j \left(\frac{\beta}{\pi}\right)^{\frac{3}{2}} \exp\left(-\beta\left(|\vec{v}_j|^2 - |\vec{v}_d|^2\right) - |\vec{v}_j||\vec{v}_d|\cos\theta\right) \tag{1.16}$$

1.3.2 Debye Shielding

That plasma dynamics will change in response to electric fields is clear on an intuitive level. For instance, the coulomb force tells us that in response to a spherical positive probe immersed in the plasma, electrons will proliferate around it forming a shielding cloud. In a cold plasma the shielding cloud will contain exactly the opposite charge carried by the probe, and beyond the radius of the cloud will shield the probe perfectly by Gauss' law. However if we consider electrons of finite temperature, it is clear that they will be able to escape the shielding cloud when the shielded potential is around $k_B T_e$. Therefore, the radius of the electron shielding cloud will extend only up to the point where the shielded potential is of order $k_B T_e$. This situation is referred to as 'Debye shielding' [32]. To quantify the length-scale over which Debye shielding takes place and the degree to which potentials are shielded in a plasma, we apply the Poisson equation to calculate the effective potential, $\phi(r)$, around a spherical probe immersed in the plasma. For simplicity, we shall assume a quasi-neutral plasma with a Boltzmann distribution of ions and electrons. We shall also make a weak coupling approximation so that $\frac{e\phi(\vec{r})}{k_b T_{i,e}} \ll 1$. Writing equation 1.13 with the Laplacian in spherical polars ($r = 0$ at the grain) and taking the system spherically symmetric, we obtain [15]:

$$\frac{1}{r^2}\frac{d}{dr}\left(r^2\frac{d\phi(r)}{dr}\right) = \frac{n_0 e^2 \phi(r)}{\varepsilon_0}\left(\frac{1}{k_b T_i} + \frac{1}{k_b T_e}\right) \tag{1.17}$$

$$\frac{d^2\phi}{dr^2} + \frac{2}{r}\frac{d\phi}{dr} = \frac{\phi(r)}{\lambda_D} \tag{1.18}$$

where

$$\lambda_D^2 = \frac{\varepsilon_0}{n_0 e^2\left(\frac{1}{k_B T_i} + \frac{1}{k_B T_e}\right)} \tag{1.19}$$

Equation 1.18 has an analytic solution, the Dëbye-Huckel potential [39]:

$$\phi(r) = \phi_p \frac{R_p}{r} \exp\left(\frac{R_p - r}{\lambda_D}\right) \tag{1.20}$$

λ_D, sometimes called the linearized Debye length, is the characteristic length scale over which shielding occurs. Therefore, charges on a scale $\ll \lambda_D$ are not shielded and they're potential falls off as $\frac{1}{r}$ [39]. For objects $< \lambda_D$ the Dëbye-Huckel potential is often used (see section 2.2.2) [17] Intuitively, we can extend equation 1.19 to separate the shielding responses by the ions and electrons. We therefore define the ion and electron Debye lengths:

$$\lambda_{Di}^2 = \frac{\varepsilon_0 k_B T_i}{n_0 e^2} \quad \lambda_{De}^2 = \frac{\varepsilon_0 k_B T_e}{n_0 e^2} \tag{1.21}$$

$$\frac{1}{\lambda_D^2} = \frac{1}{\lambda_{Di}^2} + \frac{1}{\lambda_{De}^2} \tag{1.22}$$

The ion and electron temperatures in the scrape off layer of a Tokamak plasma are typically on the same order of magnitude, so shielding is not dominated by either species [38]. The preceding analysis has drawbacks for the study of dusty plasmas, namely the weak coupling approximation is invalid for dust[15], [11]. Despite this, λ_D is still a commonly used length scale in the Dusty plasma literature. We must be wary how we apply it though.

Chapter 2

Charging by Collection

2.1 The Basic Plasma Surface Interaction

Plasmas are often thought of as comprising of an electron fluid and an ion fluid, the 'two fluid' model. Since the electrons are on the order 1×10^3 less massive than the ions, their thermal velocities are significantly greater and so an object immersed in a plasma experiences a rapid collection of electrons at its surface, gaining a negative charge. There is also an ion flux onto the grain, so that the ambipolarity condition dictates that the grain will reach a steady state potential when the electron and ion currents balance. This potential is referred to as the 'floating potential'. Debye shielding of this potential occurs as discussed in section 1.3.2. Applying the preceding model to a dust grain, one would expect the dust grain potential to be of the Dëbye-Huckel form. However, this simplified model breaks down when the dust size $\sim \lambda_{De}$ as the potential is complicated by the presence of the sheath 2.1.1. Unfortunately in SOL $\lambda_{De} \sim 1 \times 10^{-5} m$ and the average dust grain radius,a, is usually around a micrometer (see figure 2.1) so that in order to describe the physics of the dust plasma interaction adequately, it is necessary to introduce the concept of the sheath [30].

2.1.1 The Sheath, Pre-Sheath and Bohm Criterion

The shielding of the potential of a charged probe of radius a in a plasma is much researched and surprisingly incompletely understood when a is on the same scale or much larger than λ_{De}. In the opposite limit, the potential tends to $\frac{1}{r}$ as shielding takes place on the scale λ_{De}. If we take $\lambda_{De} \to 0$, it is found that the plasma surface interaction decomposes into a two scale problem consisting of a collision free sheath and a quasi-neutral presheath. Assuming a negatively charged probe, the electron density very close to the probe is reduced

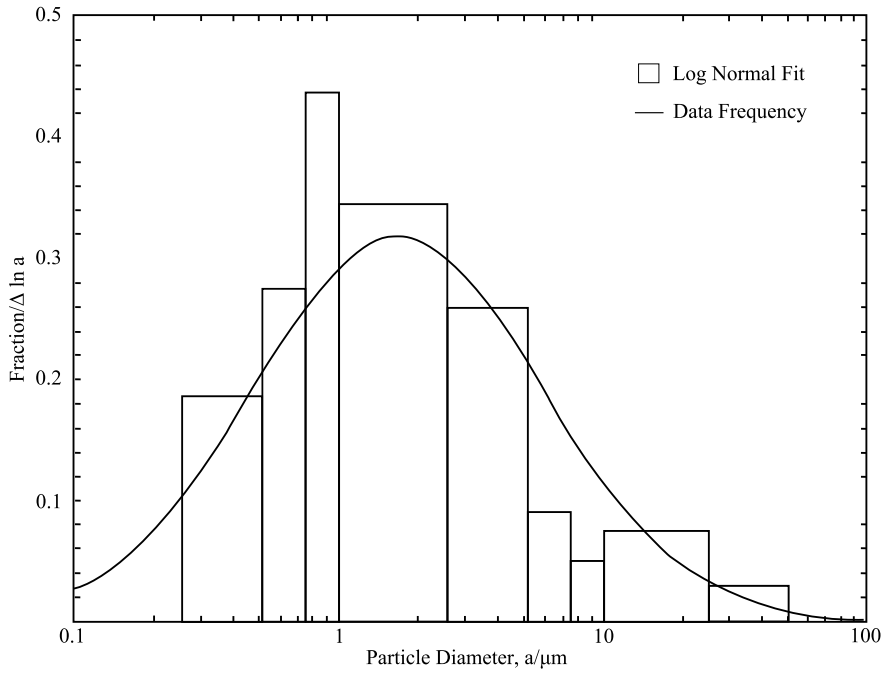

Fig. 2.1 Count based distribution of DUST obtained from behind the divertor targets of ASDEX upgrade with radius a [30]

substantially resulting in a positive space charge region; the sheath. The sheath extends to a scale $\approx \lambda_{De}$ subsequently shielding the potential to a varying degree depending on the scale of the probe, it's floating potential and the temperature. Unfortunately, this simple situation is complicated by significant ion losses due to absorption at the probe surface, rendering sheath formation impossible unless the 'Bohm criterion' is fulfilled. The essence of this condition is that in order to enter the sheath, ions must have velocity greater than or equal to the ion sound speed, C_s. Such ion velocities cannot derive from thermal motion alone and so the presence of a space region $L \gg \lambda_{De}$ containing an accelerating potential for the ions has been postulated and subsequently observed experimentally. This is the presheath. The ion velocity at the presheath-sheath boundary is often taken to be equal to C_s (see below), implying the presence of a discontinuity at the boundary informing the two scale formulation of the problem [27]. A simplified analysis of this situation in the case of a perfectly absorbing planar wall is expounded below [35]

$$C_s = \sqrt{\frac{k_B\left(\gamma T_i + T_e\right)}{m_i}} \tag{2.1}$$

In order to theoretically illustrate the existence of the sheath, presheath and Bohm criterion, some simplifying assumptions are made, namely: the plasma is assumed quasi-neutral,

collisionless, isothermal and unmagnetized with ambipolar flow $(v_i = v_e = v)$ and singly charged ions. The collisionless assumption is good for the SOL where the mean free path is $\sim 10cm$, $1000\times$ smaller than the length over which shielding takes place λ_D [40]. The perfectly absorbing planar wall scenario means that the ion distribution will not have a Bolztmann factor due to wall losses and the situation is effectively 1d. The unmagnetized assumption simplifies the equation of motion and the isothermal situation implies that the adiabatic index, $\gamma = 1$ and that the ideal gas law, $P_{i,e} = n_{i,e}k_B T_{i,e}$ may be used. This assumption, whilst not applicable to the SOL, is used because it simplifies the analysis enormously and the essential physics is the same as the full problem. We begin by illustrating the existence of a discontinuity. Beginning in the quasi-neutral plasma and including ionizations, ions and electrons are produced at the same rate, Θ, giving a continuity equation 2.2.

$$v\frac{dn}{dx} + n\frac{dv}{dx} = \Theta \tag{2.2}$$

Both species are subject to three fluid forces.

1. Pressure force: $\dfrac{-dp_i}{dx}$

2. Electrostatic force: $-nq\dfrac{d\phi}{dx}$

3. Effective drag due to ionization: $-mv\Theta$

The drag force can be justified as follows. If ion electron pairs are assumed to be produced at rest, since the plasma is assumed isothermal, the momentum of the new ion and electron will on average after a short time become $m_{i,e}v_{i,e}$ respectively. On average then the momentum of each fluid particle ignoring the new ion electron pair is reduced by that amount respectively. Thus it is seen that ionization creates a drag force on the fluid. The total drag will simply be the drag for 1 ionization multiplied by the rate of ionization. The momentum of a fluid is given by $nmv\frac{dv}{dx}$, and force balance for each species is obtained by equating this to the sum of the three forces. An overall fluid momentum equation can be written by summing the contributions from both species and since the electron mass is negligible compared to the ion mass, terms proportional to m_e are neglected. Rewriting the pressure using the ideal gas law then leads to equation 2.3

$$nmv\frac{dv}{dx} = -mC_s^2\frac{dn}{dx} - mv\Theta \tag{2.3}$$

Where $C_s^2 = \frac{nk_B(T_i+T_e)}{m_i}$ in the isothermal scenario. Defining the mach speed, $M = \frac{v}{C_s}$, subbing in equation 2.2 and rearranging results in:

$$\frac{dM}{dx}\left(n - nM^{-2}\right) = -\frac{\Theta}{C_s}\left(M^{-2}+1\right) \tag{2.4}$$

Rearranging gives equation 2.5 which implies the existence of a discontinuity at $|M| = 1$, the inference being that the initial assumptions break down at this point, suggesting that $v < C_s$ in the quasi-neutral region. This region shall be denoted the 'presheath' and the region beyond is named 'sheath'.

$$\frac{dM}{dx} = \frac{\Theta\left(1+M^2\right)}{C_s n\left(1-M^2\right)} \tag{2.5}$$

The sheath boundary shall now be analysed by probing the boundary on the sheath side region, formulating the Poisson equation. At this point it is convenient to introduce the following normalized variables:

$$X = \frac{x}{\lambda_{De}} \quad \Phi = -\frac{e\phi}{k_B T_e} \quad \theta = \frac{T_i}{T_e} \quad N_{i,e} = \frac{n_{i,e}}{n_0} \tag{2.6}$$

Defining the potential at the sheath edge $\phi_s = 0$, with the normalised variables, the electron density is simply:

$$N_e = N_s \exp((\Phi)) \tag{2.7}$$

Working on the sheath side and so on scales λ_{De}, ionizations may be neglected and ion continuity at the boundary is simply $n_i v_i = n_s v_s$. With normalised variables continuity becomes:

$$N_i = \frac{N_s M_s}{M} \tag{2.8}$$

At a point in the sheath where the potential is $\phi(x)$ and the ion velocity is v_i, ion force balance gives:

$$\frac{d}{dx}\left(\frac{1}{2}m_i v_i^2 + e\phi(x) + k_B T_i \ln[n_i]\right) = 0 \tag{2.9}$$

Integrating from a point in the sheath up to the boundary, with $\phi_s := 0$ where the velocity is v_s, produces equation 2.10.

$$\frac{1}{2}m_i\left(v_i^2 - v_s^2\right) + e\phi(x) + k_B T_i \ln\left(\frac{n_i}{n_s}\right) = 0 \tag{2.10}$$

Ion continuity at the sheath edge gives $n_i = \frac{n_s v_s}{v_i}$, where the quantities with s subscript are taken on the sheath side of the boundary. In steady state at Substituting in the normalised variables and substituting in for C_s^2 gives:

$$M^2 = M_s^2 + \frac{2}{1+\theta}\left(\Phi(X) - \theta \ln\left[\frac{N_i}{N_s}\right]\right) \tag{2.11}$$

Poisson's equation can be written in terms of equations 2.7, 2.10 and 2.11.

$$\frac{d^2\Phi(X)}{dX^2} = N_s\left\{1 + \frac{2}{M_s^2(1+\theta)}\left[\Phi(X) - \theta \ln\left(\frac{N_i}{N_s}\right)\right]\right\}^{-\frac{1}{2}} - \exp(-\Phi) \tag{2.12}$$

Very close to the sheath edge where $\Phi(X) \ll 1$, the normalised ion density $N_i \approx N_e = N_s \exp(-\Phi)$ by ion continuity. In that limit, equation 2.12 reduces to:

$$\frac{d^2\Phi(X)}{dX^2}|_{X\approx X_s} = N_s\left(1 + \frac{2\Phi(X)}{M_s^2}\right)^{-\frac{1}{2}} - \exp(-\Phi(X)) \tag{2.13}$$

Taylor expanding about the sheath edge produces equation 2.14. If the situation is assumed to reach a steady state, then oscillatory solutions are to be avoided and so $M_s^2 \geq 1$. In other words, the ion velocity in the sheath must satisfy the Bohm criterion: $v_s \geq \sqrt{\frac{K_B(T_e+T_e)}{m_i}}$. However, equation 2.5 implied that the velocity in the presheath was restricted to the opposite inequality. We therefore conclude that at the sheath edge, the ion velocity is equal to the ion sound speed. Whenever the sound speed is reached, a shock is formed, so the Bohm criterion is the origin of the discontinuity noted previously. This is denoted the Bohm speed, U_B. More generally, this conclusion can be reached in the non-isothermal case applicable for a Tokamak with the full ion distribution. Riemann [27] performs the analysis.

$$\frac{d^2\Phi(X)}{dX^2}|_{X\approx X_s} \approx \frac{N_s}{M_s^2}\left(M_s^2 - 1\right) + O\left(\Phi^2\right) \tag{2.14}$$

2.2 Dust Grain Charging

Two main approaches to calculating the floating potential of a dust grain immersed in a plasma due to charge collection shall be review; the Orbital Motion (OM) family of theories and the Radial Motion theory (ABR) approach valid for cold ions [17]. OM in it's complete form assumes Maxwellian ions and electrons in a two fluid approximation explicitly calculating the ion trajectories right up to the grain. However, since the full OM problem is very difficult to solve and solutions are only available in a limited number of cases, a restricted

OM theory, OML, is very often used. The 'L' stands for 'limited' and refers to the fact that the ion current is assumed to be limited by the angular momentum of the ions. By contrast with full OM, OML models are not full physical theories because they do not calculate ion trajectories explicitly and do not include the sheath. As a result they do not contain explicit dependence on dust grain size. This will be expounded on in section 2.2.2. ABR on the other does include sheath physics to a degree, as the Poisson equation is integrated from the bulk plasma right up to the grain. As a result the ABR floating potential contains explicit dependence on the radius of the dust grain. ABR is included despite not being appropriate for Tokamak conditions, since it is a complete theory which explicitly includes the ion trajectories onto the grain (they're radial) and provides an accurate limiting case which highlights the shortcomings of OML. Despite OMLs shortcomings it is by far most prolific model used in Tokamak literature and so it shall be explored thoroughly. In particular it finds practical use in the Tokamak dust transport codes DTOCKS and DUSTT (see Chapter 3

2.2.1 Radial Motion Theory (ABR)

As discussed in 2.1.1, an object immersed in a plasma will experience a flux of ions and electrons, consequently charging by collection. The 'floating potential' is reached when the electron and ion currents onto the object balance, $I_i + I_e = 0$, and a steady state is reached. ABR assumes cold ions and Maxwellian electrons 1.12 obeying a Boltzmann distribution 1.15 Consider an ion approaching a dust grain of radius a centred on $r = 0$

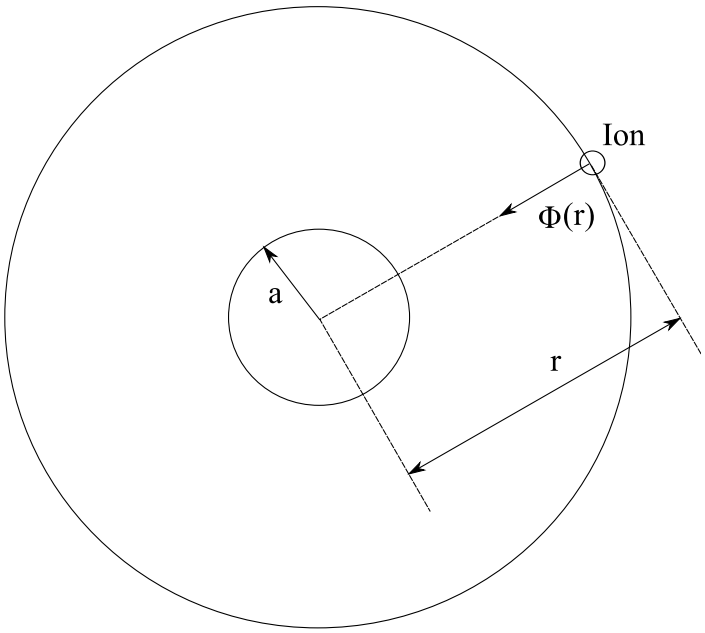

Fig. 2.2 And ion approaches a dust grain of potential $\Phi(r)$ radially

from the quasi-neutral bulk plasma (figure 2.2). Since the ions are cold $v_{i,\infty} = 0$, and the assumption of a quasi-neutral bulk implies that there are no potentials in this region, energy conservation gives:

$$v_i(r) = \left(-\frac{2e\phi_r}{m_i}\right)^{\frac{1}{2}} \tag{2.15}$$

Then the ion current through a spherical shell at radius r is:

$$I_i(r) = 4\pi r^2 n_i(r)\, e \left(-\frac{2e\phi_r}{m_i}\right)^{\frac{1}{2}} \tag{2.16}$$

It is computationally expedient to follow Kennedy and Allen ([16]) and introduce the following normalized variables.

$$X = \frac{r}{\lambda_{De}} \quad \Phi = -\frac{e\phi}{k_B T_e} \quad \phi = \frac{T_i}{T_e} \quad A = \frac{a}{\lambda_{De}} \quad N_{i,e} = \frac{n_{i,e}}{n_0} \quad \mu = \frac{m_i}{m_e} \tag{2.17}$$

$$J = \frac{I_i}{4\pi\lambda_{De}^2 n_0 e\sqrt{\frac{2k_B T_e}{m_i}}} \tag{2.18}$$

We can then write the ion density as $n_i = n_0 J\Phi^{-\frac{1}{2}}X^{-2}$ and substituting this and the Boltzmann electron density into the spherically symmetric Poisson equation leads to equation 2.19. Integrating the Poisson equation will result in $\phi(r)$ and subsequently also the normalized form $\Phi(X)$.

$$\frac{d}{dX}\left[X^2\frac{d\Phi}{dX}\right] = J\Phi^{-\frac{1}{2}} - X^2\exp(-\Phi) \tag{2.19}$$

Assuming a negatively charged grain we expect the electron distribution to be adequately approximated by the Boltzmann law (see subsection 1.3.1). Since the potential is repulsive for the electrons, we assume a Maxwellian distribution right up to the grain. Subsequently the electron current is found by taking the first velocity moment of the Maxwellian velocity distribution, substituting in the Boltzmann law, multiplying by the surface area of the grain and multiplying the electric charge e. The core of this calculation is the same as for the one way particle flux given by equation 1.11. The electron current I_e is then found to be:

$$I_e = -e\pi a^2 n_0 \exp(-\Phi)\left(\frac{8k_B T_e}{m_e}\right)^{\frac{1}{2}} \tag{2.20}$$

Rearranging equation 2.18 for I_i and equating with equation 2.20 gives 2.21, the floating condition which, together with $\Phi(X)$ allows determination of the floating potential for a

particular A.

$$\frac{J}{A^2} = \sqrt{\frac{\mu}{4\pi}} \exp\left(-\Phi_d^f\right) \tag{2.21}$$

It will be apparent later that the re-arranged form of equation 2.21 given below will be more useful.

$$\Phi_d^f(A) = \frac{1}{2} \ln\left(\frac{A^4 \mu}{4\pi J^2}\right) \tag{2.22}$$

Equation 2.19 is a second order differential equation requiring two boundary boundary conditions if it is to be integrated: $\frac{d\Phi(X)}{dX}|_{X_b}$ and Φ_b where X_b is the boundary of integration. Integration shall be performed from far within the plasma in the quasi-neutral region up to the grain. The quasi-neutral solution is termed the 'plasma solution'. We obtain the boundary conditions as follows. $\frac{d\Phi}{dX}|_{X_b}$: in the quasi-neutral plasma the normalised electron and ion densities are approximately equal to unity. This implies that the Laplacian term is very small compared to unity, therefore the 'plasma' solution is obtained by setting the Laplacian term in equation 2.19 equal to zero. Upon rearranging, equation 2.23, the plasma solution, is obtained [12].

$$X = \frac{J^{\frac{1}{2}} \exp\left(\frac{\Phi}{2}\right)}{\Phi^{\frac{1}{4}}} \tag{2.23}$$

In order to obtain $\frac{d\Phi_b}{dx}$, equation 2.23 is differentiated:

$$\frac{d}{dX}\left(XJ^{-\frac{1}{2}}\right) = \frac{d}{dX}\left(\frac{\exp\left(\frac{\Phi}{2}\right)}{\Phi^{\frac{1}{4}}}\right) \tag{2.24}$$

$$\frac{d\Phi}{dX} = \frac{4\Phi^{\frac{5}{4}}}{J^{\frac{1}{2}}} \frac{\exp\left(-\frac{\Phi}{2}\right)}{(2\Phi - 1)} \tag{2.25}$$

By factoring out X using equation 2.23, the first boundary condition is obtained.

$$\frac{d\Phi}{dX} = \frac{2X\Phi^{\frac{3}{2}} \exp(-\Phi)}{J\left(\Phi - \frac{1}{2}\right)} \tag{2.26}$$

In order to derive Φ_b, it is necessary to quantify the acceptable boundary values X_B. The X_b are arbitrary points where the plasma solution is valid. Since the plasma solution is valid only when the Laplacian term of equation 2.19 is small compared to the other two terms, may take one of the left hand terms and form an inequality, for instance, equation 2.27.

$$\frac{d}{dX}\left(X^2 \frac{d\Phi}{dX}\right) \ll J\Phi^{\frac{1}{2}} \tag{2.27}$$

Substituting in equation 2.26 and differentiating then produces:

$$\frac{6X^2\Phi^{\frac{3}{2}}\exp(-\Phi)}{J\left(\Phi-\frac{1}{2}\right)}+\frac{2X^4\Phi^2\exp(-2\Phi)}{J^2\left(\Phi-\frac{1}{2}\right)^2}\left(3-2\Phi-\frac{2\Phi}{\left(\Phi-\frac{1}{2}\right)^2}\right)\ll J\Phi^{\frac{1}{2}} \tag{2.28}$$

Substituting in equation 2.23 and simplifying leads to:

$$\frac{4\Phi^{\frac{3}{2}}(2\Phi+1)(2\Phi-3)}{(2\Phi-1)^3}\ll J \tag{2.29}$$

By introducing an arbitrarily large parameter γ, we can may re-write equation 2.29 as an equality giving a relationship between J and the boundary value Φ_{X_b}, equation 2.30.

$$\frac{J}{\gamma}=\frac{4\Phi_b^{\frac{3}{2}}(2\Phi_b+1)(2\Phi_b-3)}{(2\Phi_b-1)^3} \tag{2.30}$$

The boundary value Φ_b is obtained by arbitrarily choosing J and solving equation 2.30 numerically [15]. The allowed boundary values are plotted in figure 2.3 Before outlining the

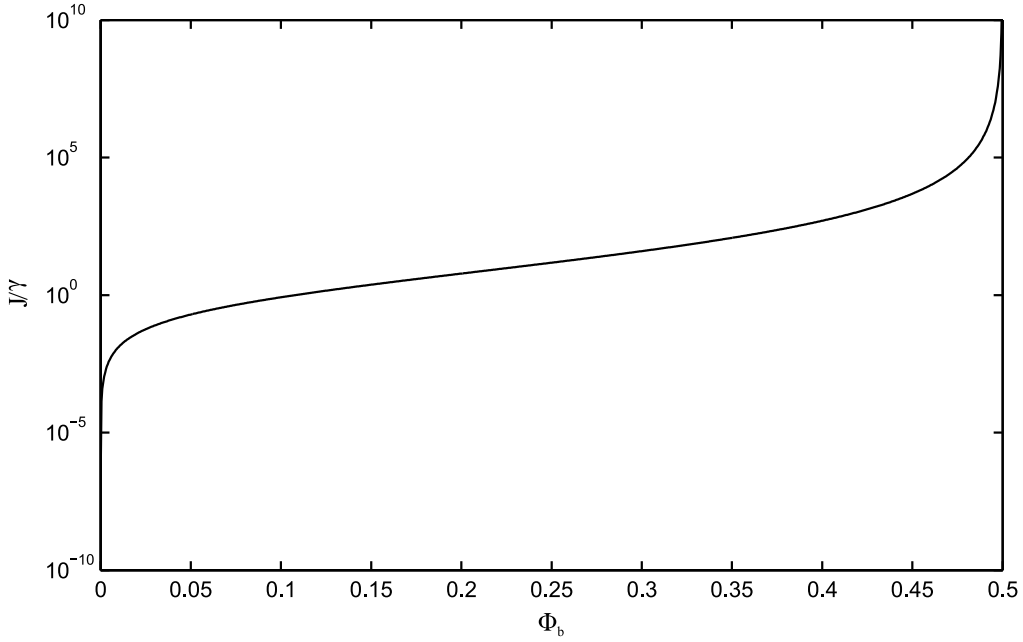

Fig. 2.3 The allowed boundary potentials Φ_b for a given $\frac{J}{\gamma}$, with γ and arbitrarily large parameter

numerical procedure for determining the ABR floating potential and discussing its conse-

quences, the general procedure shall be elucidated. Equation 2.19 is integrated for varying values of J with the boundary conditions and initial point computed as described. This produces a series of Φ_X curves for varying J 2.4. In the context of a dust grain of radius A, $\Phi(X)$ is the potential due to the grain at a normalised distance of $X-A$ for a certain value of J. Radii within A are redundant. The point on any potential curve at $X=A$ corresponds to the floating potential of the grain at that value of J. The solution, containing two unknowns, can be used to produce a function $\Phi_d^f(A)$ by combining with equation 2.22, which matches grain radius parameters to specific J values. The result is figure 2.5, computed for a D+T plasma mix.

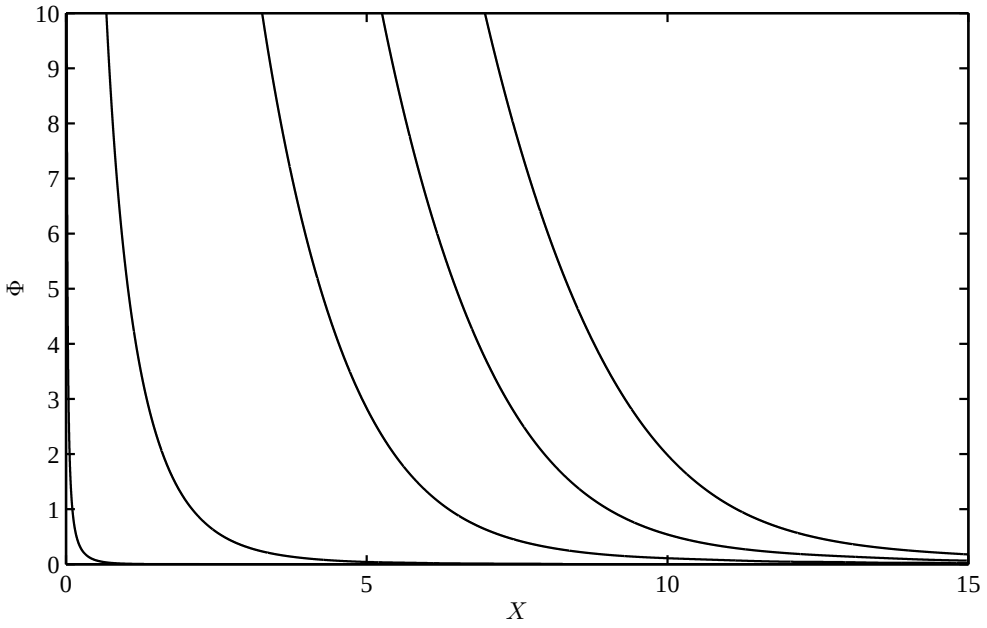

Fig. 2.4 Potential curves for the following selections of normalised current densities: $0.1, 5, 30, 55, 80$.

Figures 2.4 and 2.5 where produced using 'MATLAB'. The numerical solving function 'vpasolve' was applied to equation 2.30 to obtain $\Phi_b(J)$, and the integration of equation 2.19 was computed using 'ode45', which implements a 4th and 5th order Runga-Kutta formula (seečitepode45). Since ode45 can only handle first order equations, equation 2.19 was first converted into a system of two first order equations. This can be achieved by defining the variables $\Phi_1(X) = \frac{d\Phi(X)}{dX}$ and $\Phi_2(X) = J\Phi_1^{-\frac{1}{2}}(X)X^{-2} - \exp[-\Phi_1(X)] - 2X^{-1}\Phi_2(X)$. In addition it was found that ode45 becomes unstable when integrating 'backwards' so a change of variables was made in order to effectively integrate forwards in X. Rather than being explicitly calculated, it is more accurate to say that $\Phi_d^f(A)$ was 'generated'. More

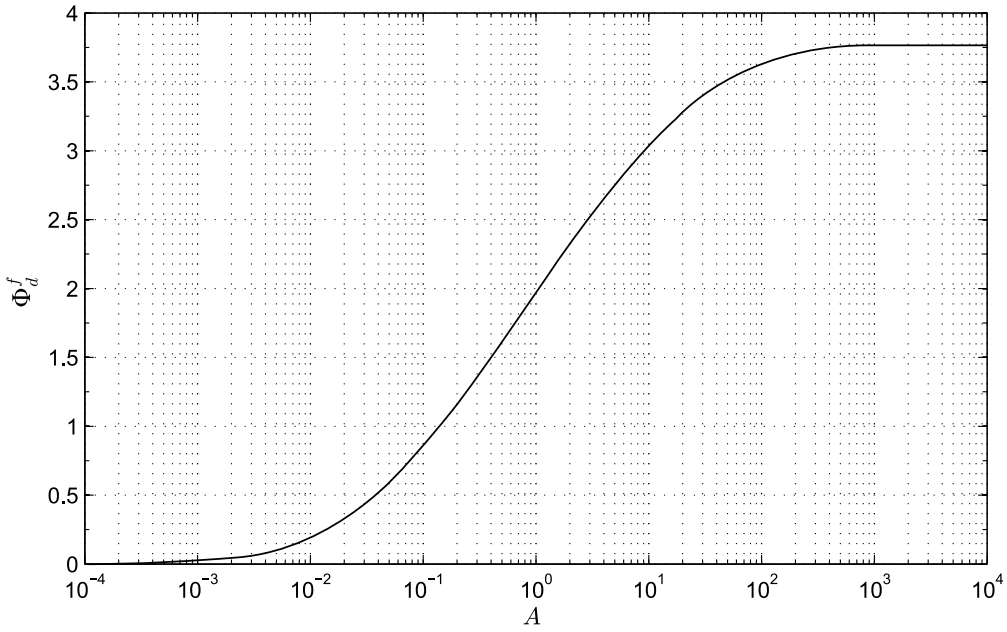

Fig. 2.5 Floating potential as a function of grain radius computed with ABR theory.

precisely, the function $\Phi(X)$ as a function of J and equation 2.22 were overplotted for each iteration of J and the value of X which corresponded to the point of intersection between the two curves gave $\Phi_d^f(A)$. Figure 2.6 illustrates this procedure graphically for a few points. Ideally the point of intersection would have been obtained by fitting a function to $\Phi(X)$, equating with equation 2.22 for every iteration and solving. However, a suitable fitting function was not readily apparent and so an alternative method was applied. This involved calculating the differences between the two functions on a fine grid using a shape preserving spline interpolant, finding the point at which an element in the differences vector changed sign, and picking the previous X value to be the intersection point. The accuracy of this method can be selected by setting the fineness of the grid. The spacing used to produce figures 2.4 and 2.5 was 1×10^{-2}. This is the dominant error in the calculation. 1×10^{-2} is an adequate tolerance because rather than using ABR to produce accurate values of the floating potential for Tokamak dust, the theory has been included in order to probe the behaviour of the floating potential in the cold ion limit. Looping over J generates the desired function Φ_d^f. It is important to note that it is not possible to perform the above calculation for a pre-selected value of A since J and A constrain one another and it is not possible to compute the $\Phi(X)$ curves without pre-selecting J. However, once $\Phi_j^f(A)$ has been generated, the floating potential for arbitrary grain radius can be obtained by interpolation or estimated graphically on figure 2.5. All of the above subtleties are documented in Appendix A where

the full code is included and extensively annotated. The numerical results show that the

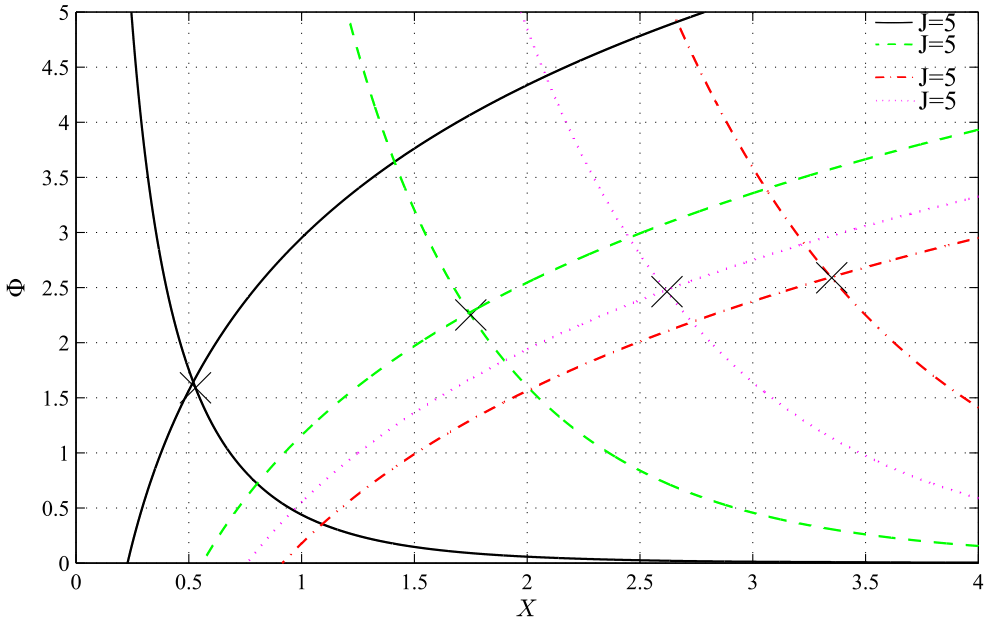

Fig. 2.6 Graphical example of the determination of the ABR floating potenial for 4 values of normalised grain radius marked by crosses.

ABR model is asymptotic in the small and large grain limits. The asymptote values are 0 and 3.80 for Φ_d^f.

2.2.2 Orbital Motion Limited (OML)

OML and its modifications are the simplest and perhaps most widely used charging models and belong to a class of theories known as Orbital Motion (OM). Unlike ABR, OM theories consider both hot ions and electrons. OML shall be presented in various guises in this paper. First of all the basic theory, applicable to negatively charged dust grains, is described in this section. The three subsequent sub-sections detail modifications addressing some of OML's shortcomings. It should be said at the outset, that the justification for these particular modifications comes not from theory but from experiment. In Chapter 3 the DTOCKS and DUSTT codes OML based charging mechanisms are reviewed. These take into account some of the various electron emission processes leading to the aforementioned positive grains. Unlike ABR, OML deals with both hot ions and electrons so it is immediately more applicable to a Tokamak. OML is theoretically questionable on many counts. One of the most striking features of OML is that it doesn't calculate or assume any ion trajectories. In this sense, it

is not a complete theory unlike the ABR model which assumes radial motion of the incoming ions. Secondly OML assumes a negatively charged grain when in fact there are many circumstances under Tokamak conditions when the grain charges positive (see 3). The dust transport codes DUSTT and DTOCKS both modify OML to rectify this (see 3). Another issue is that, as we shall see in 2.2.4, the assumption that grazing ions are collected is invalidated for $\frac{a}{\lambda_D} \ll 1$ by the presence of an 'absorption radius', $\frac{a_{ab}}{\lambda_D}$ where $a_{ab} \neq a$. Again, OML may be modified to account for this phenomenon 2.2.4. Finally, since OML contains a fixed Maxwellian distribution used to calculate the electron and ion fluxes onto the grain, the theory is invalid when flows are present, as in a Tokamak. A version of OML with a shifted Maxwellian shall be presented in subsection 2.2.5. It is assumed that the grain has rapidly charged negative by electron collection, and only ion collection need be considered. Figure 2.7 illustrates the situation. We consider ions approaching from infinity with velocity v_∞. Ions which have a certain critical parameter η_c will follow an unspecified trajectory which just grazes the surface of the grain, and ions with parameter less than η_c will be collected at the surface grain.

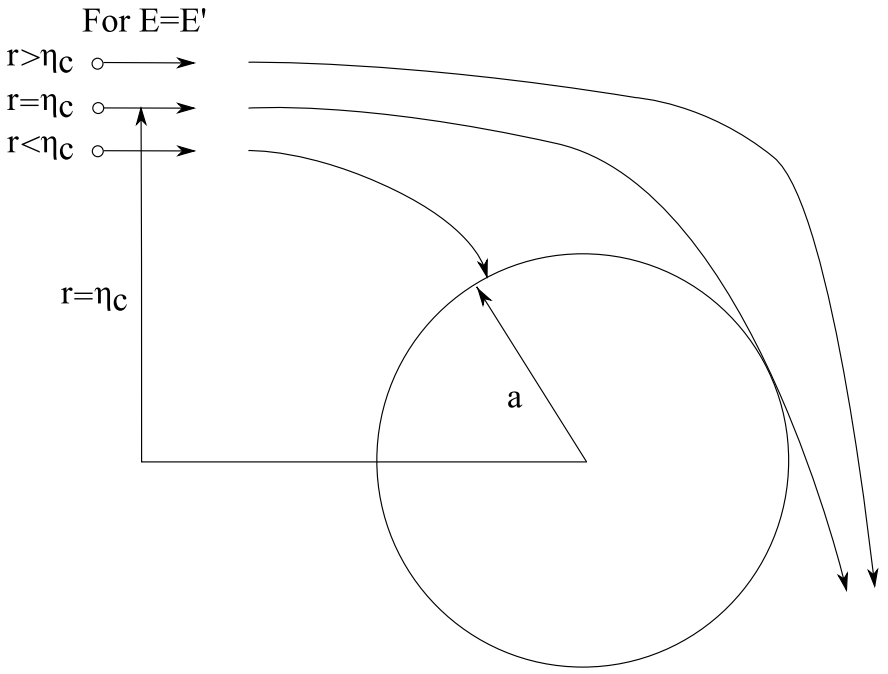

Fig. 2.7 The allowed boundary potentials Φ_b for a given $\frac{J}{\gamma}$, with γ and arbitrarily large parameter

Following Kennedy and Allen ([17]), we begin by assuming a Maxwellian plasma and a spherical grain, implying that the situation is spherically symmetric. with This allows us

to assume angular momentum 2.31 and energy 2.32 conservation respectively

$$m_j v_\infty \eta_c = m_j v_j a \tag{2.31}$$

$$\frac{1}{2} m_i v_\infty^2 = \frac{1}{2} m_i v_i^2 + e\phi_d \tag{2.32}$$

Where m_j, ϕ_d, v_∞ are the mass of species j, potential at the surface of the dust grain and the velocity in the bulk plasma. We assume 'ambipolar' flow so that in the bulk $v_i = v_e = v_\infty$ [22]. η_c is the critical parameter for which particles follow an unspecified trajectory which is at some point tangential to the dust grain complete with zero radial velocity with respect to the grains radius. We may calculate the effective area upon which ions are collected by first combining equations 2.31 and 2.32 to derive an expression for η_c. Subsequently we straightforwardly obtain expression 2.33 for the effective cross section of collection for the ion current, σ_i.

$$\sigma_i = \pi a^2 \left(1 - \frac{2e\phi_d}{m_i v_\infty'^2}\right) \tag{2.33}$$

From the exposition in 2.1.1 we know that ion collection on the negatively charged grain will result in the formation of a sheath. It was argued that ions must enter the sheath with $v_i = U_B$, so we would expect the presence of a potential barrier against the ion collection during formation of the sheath. OML ignores this complication. This simplification is encoded in the initial 'grazing' assumption and shall be addressed in 2.2.4 by the inclusion of the aforementioned 'absorption radius'. In addition it is assumed that the ion distribution remains Maxwellian right up to the grain. This assumption is not justifiable theoretically since Tokamak plasmas are generally considered collisionless although despite this, the Maxwellian assumption is a common approximation. The main advantage of this simplification is computation expediency, very important when one considers that the dust grain charge routine is one of many aspects to a dust transport code like DTOCKS or DUSTT (see 3) for it allows one to obtain the ion flux simply by integrating the Maxwellian from the bulk right up to the grain. Before proceeding it's worth noting that since the dust grain number density is far inferior to the plasma number density, if we assume that the reactor is operating at steady state we may assume that the presence of dust grains in the edge plasma has little affect on the plasma, and since it has been shown that Maxwellian distributions are good approximations in steady plasmas, there is at least some validity to the Maxwellian via experiment. For now, the grazing condition allows us to approximate the ion current, DI_i, due to ions with velocity $v_i + dv_i$ as:

$$dI_i = \sigma_i e dv_i v_i f_m(v_i) \tag{2.34}$$

Where n_∞ is the number density far into the bulk plasma. We shall assume a quasineutral bulk so that $n_i(\infty) = (n_e(\infty) = n_\infty$. Assuming that the grain is charged negative, the minimum speed for collection is simply $v_i = 0$. Then Substituting into 2.34 the Maxwell speed distribution 1.12, and integrating over all speeds we obtain:

$$I_i = 4\pi a^2 n_0 e \left(\frac{\beta_i}{\pi}\right)^{\frac{3}{2}} \int_0^\infty dv_i^{'} \left[v_i^{'3} - \frac{2e\phi_d v_i^{'}}{m_i} \exp\left(-\beta_i v_i^{'2}\right) \right] \tag{2.35}$$

Where

$$\beta_j = \frac{m_j}{2k_B T_j} \tag{2.36}$$

Performing the Gaussian integral leads to the ion current, I_i:

$$I_i = \pi a^2 n_0 e \left(\frac{8k_B T_i}{m_i \pi}\right)^{\frac{1}{2}} \left[1 - \Phi_{d,i}\right] \tag{2.37}$$

Where we have defined a normalised dust grain potential, $\Phi_{d,j}$ as:

$$\Phi_{d,j} = \frac{\phi_d q_j}{k_B T_j} \tag{2.38}$$

The electron current is derived the same way except that whereas the minimum collection speed for ions is just zero, since the electrons are in a repulsive potential if they are to be collected they must have speed $v_{e,min}$. Therefore the electron current is given by 2.39

$$I_e = 4\pi a^2 n_0 e \left(\frac{\beta_e}{\pi}\right)^{\frac{3}{2}} \int_{v_{e,min}}^\infty dv_i^{'} \left(v_i^{'3} - \frac{2e\phi_d v_i^{'}}{m_i} \exp\left(-\beta_e v_i^{'2}\right) \right) \tag{2.39}$$

We must be careful to ensure none of our limits diverge to infinity so they shall be written explicitly. First, label the integrals I_A and the I_B so that:

$$I_A = \int_{v_{e,min}}^\infty dv_e^{'} v_e^{'3} exp\left(-\beta_e v_e^{'2}\right) \tag{2.40}$$

$$I_B = -\int_{v_{e,min}}^\infty dv_i^{'} \left(\frac{2e\phi_d v_i^{'}}{m_i}\right) \exp\left(-\beta_e v_i^{'2}\right) \tag{2.41}$$

To evaluate I_A we integrate by parts to obtain

$$I_A = \left[-\frac{1}{2\beta_e} v_e'^2 \exp\left(-\beta_e^2 v_e'^2\right) - \frac{1}{2\beta_j^2} \exp\left(-\beta_e^2 v_e'^2\right) \right]_{v_{e,min}}^{\infty} \tag{2.42}$$

Observe that in the first term of 2.42, the upper limit converges to zero quicker in the exponential term than the squared term goes to infinity, so the upper limit is duly zero.

$$I_B = \left[\frac{v_{e,min}^2}{2\beta_e} \exp\left(-\beta_e v_e'^2\right) \right]_{v_{e,min}}^{\infty} \tag{2.43}$$

Combining 2.42 and 2.43 gives the OML electron current onto a negatively charged dust grain 2.44

$$I_e = -\pi a^2 n_0 e \left(\frac{8k_B T_e}{\pi m_e}\right)^{\frac{1}{2}} \exp\left(\frac{e\phi_d}{k_B T_e}\right) \tag{2.44}$$

Using 2.37 and 2.44, the floating condition is obtained:

$$\exp\left(-\Phi_d^f\right) = \left(\frac{\theta}{\mu}\right)^{\frac{1}{2}} \left(1 + \frac{\Phi_d^f}{\theta}\right) \tag{2.45}$$

Where the following normalised quantities are introduced:

$$\Phi_d^f = -\frac{e\phi_d}{k_B T_e} \quad \theta = \frac{T_i}{T_e} \quad \mu = \frac{m_i}{m_e} \tag{2.46}$$

It is notable that Equation 2.45 produces a result for the floating potential that is independent of grain radius, in direct contradiction to ABR theory which finds the floating potential tending to zero as the normalised dust radius tends to 0 [16] Figure 2.8 shows normalised floating potential Φ_d^f against the ratio of the ion to electron temperature θ for the OML solution. ITER's benchamark mode of operation, ELMy H-Mode, is expected to operate at approximately $\theta = 1$ [31]. Since OML does not solve the Poisson equation it gives no potential profile. Therefore, it is often assumed that the potential is of the Dëbye-Huckel form (equation 1.20). This is limited to the regime $A < 1$ after which point the effects of the sheath must be included [16]. The Dëbye-Huckel potential is plotted in figure 2.9 for various values A.

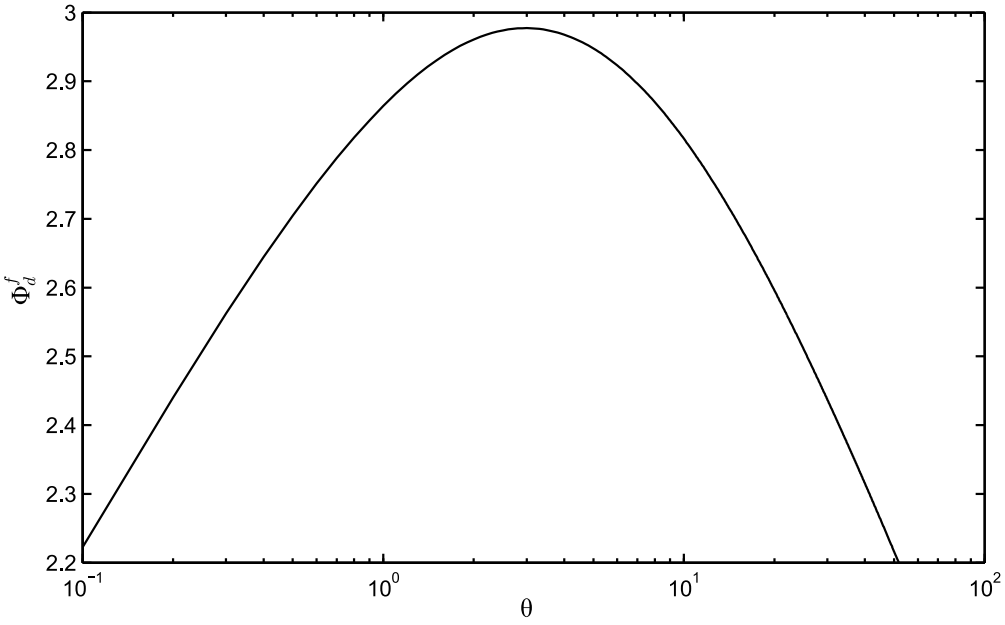

Fig. 2.8 The floating potential Φ_d^f against the normalised ion temperature θ

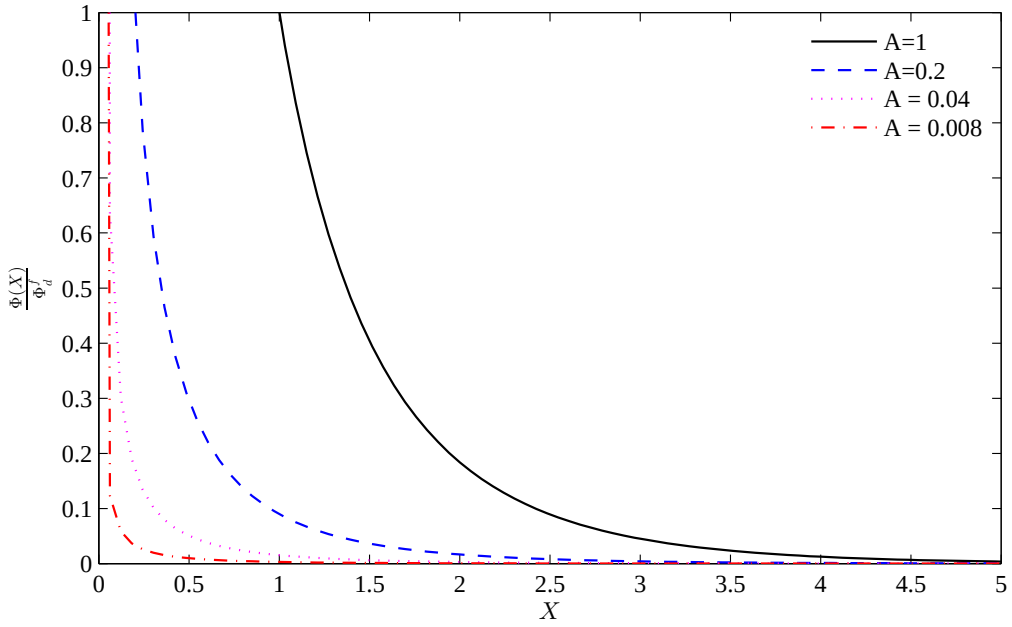

Fig. 2.9 The Dëbye-Huckel potential for various values of Normalised grain radius A.

2.2.3 The Lambert W Function - An Analytic OML Solution

The Lambert W Function $W(Z)$ is defined as the inverse function of $f(x) = x\exp(x)$ for any complex number Z so that its defining property is 2.47 [7]

$$Z = W(Z)\exp(W(Z)) \tag{2.47}$$

By multiplying equation 2.45 by $\exp(-\theta)$ and rearranging, we see that the OML floating condition can be thought of as being of the form $\Gamma\exp(\Gamma) = \kappa(\mu,\phi)$. The solution of this expression may be written as $\Gamma = W(\kappa(\mu,\theta))$. Subsequently, it is found that equation 2.48 has an analytic solution which can be written as equation 2.49

$$\left(\theta + \Phi_d^f\right)\exp\left(\theta + \Phi_d^f\right) = \sqrt{\mu\theta}\exp(\theta) \tag{2.48}$$

$$\Phi_d^f = W\left[\sqrt{\mu\theta}\exp(\theta)\right] - \theta \tag{2.49}$$

Equation 2.49 is confirmed by plotting and checking that the result matches that of figure 2.8 and indeed this is the case.

2.2.4 Modified OML (MOML)

To derive equation 2.49 it was assumed that only grains with a parameter less than the η_c are collected. However this assumption breaks down in the large grain limit, $A > 1$, due to the presence of a sheath. As discussed in section 2.1.1 the sheath occurs at a discontinuity from the pre-sheath plasma where strong electric fields accelerate electron. Bohm's postulate, that ions entering the sheath must be travelling at the Bohm speed (the sound speed) $c_s^2 = \frac{K_b(\gamma T_i + T_e)}{m_i}$ where γ is the ratio of the specific heats at constant pressure and constant volume respectively, implies the presence of potential barriers which are functions of ion energy. Taking the original OML derivation to apply strictly only in the small grain, $A < 1$ sheathless limit, we now derive an OML equation for the opposite limit which is commonly named 'MOML'. Following Willis et. al [40] we assume that all potential barriers exist at or within the sheath thereby making the sheath edge the effective grain radius. The MOML floating condition is derived by applying OML at the sheath edge. The situation is illustrated by 2.10.

Assuming a negatively charged grain, the electrons will be unaffected by the potential barriers due to the sheath since it is a region positive charge density shielding the negatively charged grain in this instance. Following Willis et. al [40] and assuming that all ions which enter the absorption radius are collected at the grain surface the ion current, equation 2.50,

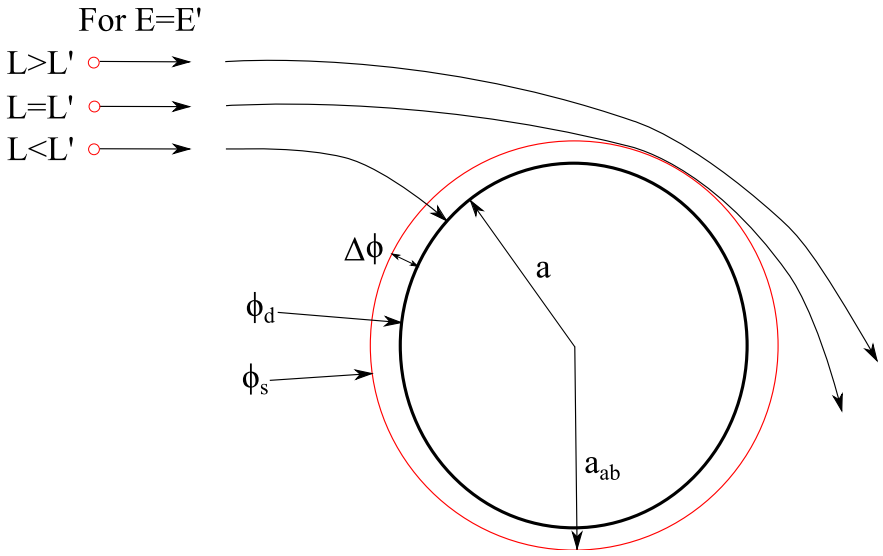

Fig. 2.10 Ions of energy E' and angular momentum L' will graze the absorption radius, a_{ab}. Ions with $L < L'$ will be collected by the grain and ions with $L > L'$ will not. ϕ_s and ϕ_d are the potentials at the sheath and dust grain edge respectively.

is obtained.

$$I_i = \pi a^2 n_0 e \left(\frac{8K_B T_i}{\pi m i_i}\right)^{\frac{1}{2}} \left[1 - \frac{e}{K_B T_i}(\phi_s)\right] \tag{2.50}$$

Substituting $\phi_d - \Delta\phi = \phi_s$ and equating with the electron current equation 2.44 and normalising as before, the floating condition is obtained.

$$\exp\left(-\Phi_d^f\right) = \sqrt{\frac{\theta}{\mu}}\left(1 + \frac{\Phi_d^f}{\theta} - \frac{\Delta\Phi}{\theta}\right) \tag{2.51}$$

In the thin sheath limit, the situation is equivalent to the planar wall in section 2.1.1 so that, with the assumption that all ions enter the sheath are collected by the grain, it is possible to estimate the potential drop across the sheath. The ion flux at the sheath edge, $\Gamma_{se}^i = n_{se}^i c_s$, is assumed to be equal the electron flux at the sheath edge, $\Gamma_{se}^e = n_{se}^e v_{se}^e$, by charge conservation. Since the electrons are still in a repulsive potential, Γ_{se}^e is just the one way particle flux in a Maxwellian distribution given by equation 1.11. Therefore, we have:

$$n_{se}^i \sqrt{\frac{k_B T_e \gamma k_B T_i}{m_i}} = \frac{1}{4} n_{se}^e \left(\frac{8k_B T_e}{\pi m_e}\right)^{\frac{1}{2}} \exp\left(\frac{e\Delta\phi}{k_B T_e}\right) \tag{2.52}$$

Making the usual assumption of a quasi-neutral pre-sheath, the above equation can be solve for $\Delta\phi$ and normalised in the usual manner to give equation 2.53.

$$\Delta\Phi = \frac{1}{2}\ln\left[\frac{2\pi}{\mu}(1+\gamma\theta)\right] \tag{2.53}$$

Substituting into equation 2.51 gives the full MOML floating condition.

$$\exp\left(-\Phi_d^f\right) = \sqrt{\frac{\theta}{\mu}}\left(1+\frac{\Phi_d^f}{\theta}-\frac{1}{2\theta}\ln\left[\frac{2\pi}{\mu}(1+\gamma\theta)\right]\right) \tag{2.54}$$

Equation 2.54 can be solved numerically in its present form or, as with the original OML formula, has an analytic solution in terms of the Lambert W function. This can be seen by rearranging to give:

$$\sqrt{\theta\mu}\exp\left(\theta-\frac{\theta}{2}\ln\left[\frac{2\pi}{\mu}(1+\gamma\theta)\right]\right) =$$

$$\left(\theta+\Phi_d^f-\frac{1}{2}\ln\left[\frac{2\pi}{\mu}(1+\gamma\theta)\right]\right)\exp\Big/\left\{\theta+\Phi_d^f-\frac{1}{2}\ln\left[\frac{2\pi}{\mu}(1+\gamma\theta)\right]\Big/\right\} \tag{2.55}$$

The solution of which is equation 2.56

$$\Phi_d^f = W\Big/\left\{\sqrt{\mu\theta}\exp\left[\beta\left(\mu,\theta\right)\right]\Big/\right\}-\beta\left(\mu,\theta\right) \tag{2.56}$$

Where $\beta\left(\mu,\theta\right)$ is defined as:

$$\beta\left(\mu,\theta\right) = \theta\left[1-\frac{2\pi}{\mu}(1+\gamma\theta)\right] \tag{2.57}$$

Willis et. al [40] have found that taking $\gamma = \frac{5}{3}$ fits the simulation data from the SCEPTIC code the best. Equations 2.56 and 2.49 are plotted in figure 2.11. Since the only fundamental difference between MOML and OML is the inclusion of potential barriers in the former, it would be expected that the MOML floating potential would be lower than the OML value for low temperatures, gradually converging to the OML value the ion temperature rise and θ heads towards and beyond unity. This is just the pattern shown in the figure which indicates that for the conditions of interest in an edge Tokamak plasma, $\theta \neq 1$, MOML offers a significant correction to the standard OML expression for large grains. In the small grain limit, MOML is expected to converge to OML since on scales $A \ll 1$ there is no sheath and so no potential barriers to ion collection, the original OML situation. So far we have developed two theories which can be applied to large and small dust grains in a stationary

plasm. Are equations 2.56 and 2.49 applicable to the SOL of a Tokamak? Unfortunately the SOL contains contains very strong plasma flows in the toroidal and poloidal directions on the order of $\neq 10^3$ and $10 Kms^{-1}$ respectively. In the next section, OML and MOML will be modified to include flow in the small and large grain limits. The resulting theories will be name SOML and SMOML where the 'S' denotes the fact that a shifted Maxwellian distribution 1.16 replaces the ordinary Maxwellian.

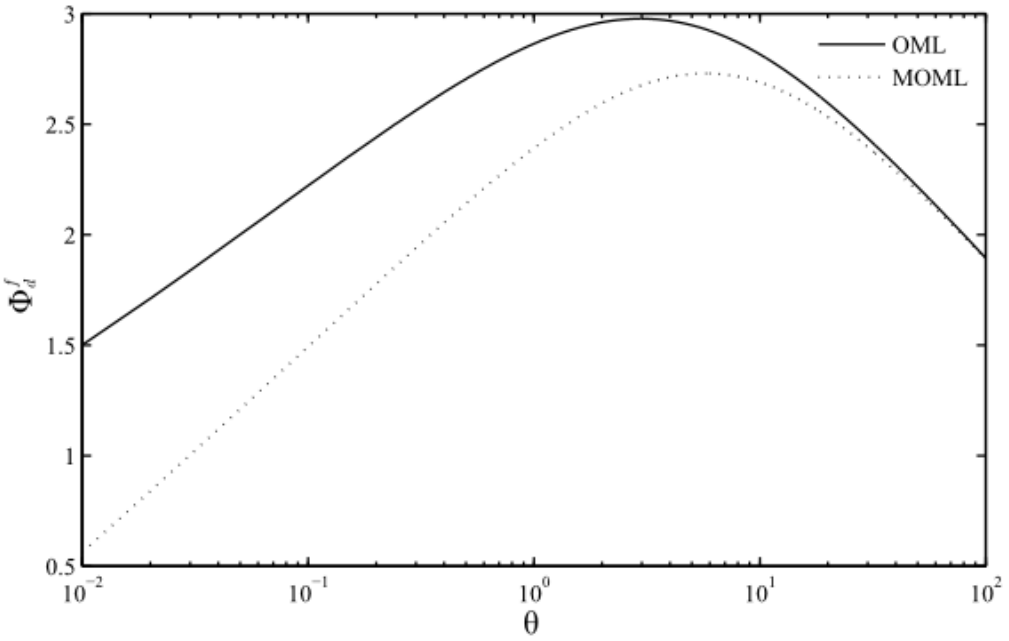

Fig. 2.11 The OML and MOML floating potentials as a function of temperature for a 50-50 D+T mix.

2.2.5 Shifted Maxwellian OML (SOML)

SOML is OML with the Maxwellian distribution replaced by the drifting Maxwellian 1.16 [18]. The fluxes onto the grain are again calculated in the usual OML method 2.2.2. The current onto the grain due to species j can be written as the integral 2.58. Substituting in the shifted Maxwellian distribution 1.16 and the OML cross section σ_j 2.33 and subsequently integrating over θ and π leads to 2.59.

$$I_j = \int_0^{2\pi} \int_0^{\pi} d\theta \sin\theta \int_{v_j^{min}}^{\infty} dv_j v_j^3 \sigma_j q_j f_j \left(v_j, \theta\right) \tag{2.58}$$

$$I_j = \Gamma_j \int_{v_j^{min}}^{\infty} dv_j \left(v_j^2 - \frac{2\phi_d q_j}{m_j} \right) \left[\exp\left(-\alpha_j^2\right) - \exp\left(-\beta_j^2\right) \right] \tag{2.59}$$

where the quantities Γ_j, α_j and β_j are defined for mathematical simplicity as:

$$\Gamma_j = \frac{v_{tj}^2}{v_d} (\pi a)^2 q_j n_j \left(\frac{m_j}{2\pi k_B T_j} \right)^{\frac{3}{2}} \tag{2.60}$$

$$\alpha_j = \frac{v_j - v_d}{v_{tj}} \quad \beta_j = \frac{v_j + v_d}{v_{tj}} \tag{2.61}$$

Where v_{tj} is the thermal velocity of species j defined as:

$$v_{tj}^2 = \frac{2k_B T_j}{m_j} \tag{2.62}$$

Expanding Equation 2.59 leads to the following Gaussian integrals 2.63, 2.64, 2.65 and 2.66

$$I_j = \Gamma_j \int_{v_j^{min}}^{\infty} dv_j v_j^2 \exp\left(-\alpha^2\right) \tag{2.63}$$

$$-\Gamma_j \int_{v_j^{min}}^{\infty} dv_j v_j^2 \exp\left(-\beta^2\right) \tag{2.64}$$

$$+\Gamma_j \frac{2\phi_d q_j}{m_j} \int_{v_j^{min}}^{\infty} dv_j \exp\left(-\beta^2\right) \tag{2.65}$$

$$-\Gamma_j \frac{2\phi_d q_j}{m_j} \int_{v_j^{min}}^{\infty} dv_j \exp\left(-\alpha^2\right) \tag{2.66}$$

Again the ion current for a negative grain is found by setting $v_j^{min} = 0$ and electron current uses the limit $v_j^{min} = \sqrt{-\frac{2e\phi_d}{m_e}}$. In the general situation of a positive grain, it is clear that when the condition $q_j\phi_d \leq 0$ is satisfied then the limit is $v_j^{min} = 0$, and when $q_j\phi_d > 0$ then $v_j^{min} = \sqrt{\frac{-2e\phi_d}{m_e}}$. With shall deal with the former case first. In order to evaluate the integrals we change the integration variables to match the term α_j or β_j in the exponential terms. For instance, term 2.63 is computed as follows.

$$I_j = v_{Tj} \int_{-\frac{v_d}{v_{Tj}}}^{\infty} d\alpha_j \left(\alpha^2 v_{Tj}^2 + 2\alpha v_{Tj} v_d + v_d^2 \right) \exp\left(-\alpha^2\right) \tag{2.67}$$

The middle term integrates trivially but the other two do not have an analytic solution so we use the standard Gaussian error function 2.68 which can evaluated numerically as the situation demands.

$$erf\,(x) := \frac{2}{\sqrt{\pi}} \int_0^x du \exp\left(-u^2\right) \quad erf\,(\infty) = 1 \tag{2.68}$$

The third term becomes:

$$v_{Tj} v_d^2 \left[\int_{-\frac{v_d}{v_{Tj}}}^{0} d\alpha_j \exp\left(-\alpha^2\right) \int_0^{\infty} d\alpha_j \exp\left(-\alpha^2\right) \right] \tag{2.69}$$

The right hand term integrates straightforwardly to $\frac{\sqrt{\pi}}{2}$ but the left term requires the error function. Since $\exp\left(-\alpha_j^2\right)$ is an even function integrating from $-\frac{v_d}{v_{Tj}} \to 0$ is equivalent to integration from $0 \to \frac{v_d}{v_{Tj}}$. We therefore make this change of limits, and write this term in terms of equation 2.68 to give:

$$\frac{\sqrt{\pi} v_{Tj} v_d^2}{2} \left[1 + erf\left(U_j\right)\right] \tag{2.70}$$

Where U_i is the drift velocity normalised with the thermal velocity.

$$U_i = \frac{v_d^2}{v_{tj}^2} \tag{2.71}$$

The first term in term 2.63 is:

$$v_{Tj}^3 \left[\int_0^{\frac{v_d}{v_{Tj}}} d\alpha_j^2 \exp\left(-\alpha_j^2\right) \right] + \int_0^{\infty} \alpha_j^2 \exp\left(-\alpha^2\right) \tag{2.72}$$

The second term is another standard Gaussian integral but the first term requires integration by parts and another application of the error function leading to:

$$\frac{\sqrt{\pi} v_{Tj}^3}{4} \left(1 + erf\left(U_j\right) - \frac{2}{\sqrt{\pi}} U_j \exp\left(-U_j^2\right)\right) \tag{2.73}$$

Putting all the pieces together we find that term 2.63 integrates to 2.74

$$\frac{\sqrt{\pi} v_{Tj}^3}{4} \left(1 + erf\left(U_j\right) - \frac{2}{\sqrt{\pi}} U_j \exp\left(-U_j^2\right)\right)$$

$$v_d v_{Tj}^2 \exp\left(-U_j^2\right) + \frac{\sqrt{\pi} v_{Tj} v_d^2}{2}\left(1 + erf\left(U_j\right)\right) \tag{2.74}$$

Terms 2.64, 2.65 and 2.66 are computed similarly, together leading to the current 2.75

$$I_j = \pi a^2 q_j n_j \left(\frac{8k_B T_j}{\pi m_j}\right)^{\frac{1}{2}} \left(\eta_1\left(U_j\right) - \eta_2\left(U_j\right)\Phi_{d,j}\right) \tag{2.75}$$

Where we have defined $\eta_1(U_i)$ and $\eta_2(U_i)$ as:

$$\eta_1(U_i) = \frac{\sqrt{\pi}}{4}\left(1 + 2U_i^2\right)\frac{erf(U_i)}{U_i} + \frac{1}{2}\exp\left(-U_j^2\right) \quad \eta_2(U_i) = \frac{\sqrt{\pi}}{2}\frac{erf(U_i)}{U_i} \tag{2.76}$$

The electron current may be written in a similar form by defining the functions $\Lambda_1\left(U_e, \Phi_{d,e}\right)$ and $\Lambda_1\left(U_e, \Phi_{d,e}\right)$ giving 2.81

$$I_e = -\pi a^2 e n_0 \left(\frac{8k_B T_e}{\pi m_i}\right)^{\frac{1}{2}} \left(\Lambda_1\left(U_e, \Phi_{d,e}\right) - \Lambda_2\left(U_e, \Phi_{d,e}\right)\Phi_{d,e}\right) \tag{2.77}$$

$$\begin{aligned}\Lambda_1\left(U_e, \Phi_{d,e}\right) = \frac{\sqrt{\pi}}{8U_e}\left(1 + 2U_e^2\right)\left[erf\left(U_e - \sqrt{\Phi_{d,e}}\right) + erf\left(U_e + \sqrt{\Phi_{d,e}}\right)\right] \\ + \frac{1}{4}\left\{\exp\left[-\left(U_e - \sqrt{\Phi_{d,e}}\right)^2\right] + \exp\left[-\left(U_e + \sqrt{\Phi_{d,e}}\right)^2\right]\right\}\end{aligned} \tag{2.78}$$

$$\begin{aligned}\Lambda_2\left(U_e, \Phi_{d,e}\right) = \frac{1}{4U_e\sqrt{\Phi_{d,e}}}\left\{\exp\left[-\left(U_e + \sqrt{\Phi_{d,e}}\right)^2\right] + \exp\left[-\left(U_e + \sqrt{\Phi_{d,e}}\right)^2\right]\right\} \\ + \frac{\sqrt{\pi}}{4U_e}\left[erf\left(U_e - \sqrt{\Phi_{d,e}}\right) + erf\left(U_e + \sqrt{\Phi_{d,e}}\right)\right]\end{aligned} \tag{2.79}$$

To summarise, for a negatively charged grain in a quasi-neutral plasma, the ion and electron SOML currents are given by equations 2.80 and 2.81 respectively [18].

$$I_i = \pi a^2 e n_0 \left(\frac{8k_B T_i}{\pi m_i}\right)^{\frac{1}{2}} \left[\eta_1(U_i) - \eta_2(U_i)\Phi_{d,i}\right] \tag{2.80}$$

$$I_e = -\pi a^2 e n_0 \left(\frac{8k_B T_e}{\pi m_e}\right)^{\frac{1}{2}} \left[\Lambda_1\left(U_e, \Phi_{d,e}\right) - \Lambda_2\left(U_e, \Phi_{d,e}\right)\Phi_{d,e}\right] \tag{2.81}$$

The above may then be combined in the usual way and solved for the Φ_d^f. The result is equation 2.82 where we have used the $\Phi_{d,i} = \frac{\Phi_d^f}{\theta}$

$$\Phi_d^f = \frac{\sqrt{mu\theta}\Lambda_1\left(U_e, \Phi_d^f\right) - \theta\eta\left(U_i\right)}{\sqrt{\mu\theta}\Lambda_2\left(U_e, \Phi_d^f\right) - \eta_2\left(U_i\right)} \tag{2.82}$$

For a positively charged grain the currents are switched because the equations 2.80 and 2.81 were derived from the same integral just with different limits selected depending upon whether the particle type, j, in question was in an attractive or a repulsive potential. Obviously electron quantities are substituted for their ion counterparts and vice versa where relevant. The internal consistency of OML and SOML taken together can be established by taking the limits of normalised drift velocity $U_j \ll 1$ and $U_j \gg 1$. For instance, we can take the former limit of equation 2.80 by Taylor expanding to first order. The error function is convergent and has a Taylor expansion computed by 2.83. We subsequently obtain 2.84

$$erf\left(z\right) = \frac{2}{\sqrt{\pi}}\sum_0^\infty \frac{(-1)^n z^{n+1}}{n!\left(2n+1\right)} = \frac{2}{\sqrt{\pi}}\left(z - \frac{z^3}{3} + ...\right) \tag{2.83}$$

$$I_i \approx \frac{\sqrt{\pi}}{4}\left(1+2U_i^2\right)\frac{1}{U_i}\left(\frac{2}{\sqrt{\pi}}U_i + O\left(U_i^3\right)\right) + \frac{1}{2}\left(1 - O\left(U_i^2\right)\right) - \frac{\sqrt{\pi}}{2}\frac{1}{U_i}\left(U_i + O\left(U_i^3\right)\right) Phi_{d,i}$$
$$= \pi a^2 e n_0 \left(\frac{8k_B T_e}{\pi m_i}\right)^{\frac{1}{2}}\left[1 - \Phi_{d,i}\right] \tag{2.84}$$

Which is just the original OML ion current 2.37. A similar analysis performed on equation 2.81 leads to the current 2.44 as expected. In the opposite limit we find that the ion and electron expressions both converge to equation 2.87, which is the formula for the current due to a mono-energetic ion or electron beam. For instance, taking the limit for the electron beam this time, the analysis goes as follows.

$$I_e = -\pi a^2 e n_0 \left(\frac{8k_B T_e}{\pi m_e}\right)^{\frac{1}{2}}\left[\frac{\sqrt{\pi}}{2}2U_e^2\frac{2}{2U_e} - \frac{\sqrt{\pi}}{2}\frac{2}{2U_e}\Phi_{d,e}\right] \tag{2.85}$$

$$= -\pi a^2 e n_0 v_d \left[1 + 2\frac{e\phi_d}{m_e v_d^2}\right] \tag{2.86}$$

And in general equation 2.86 can be written 2.87

$$I_{j,mon} = \pi a^2 q_j n_j v_d \left[1 - 2\frac{q_j \phi_d}{m_j v_d^2}\right] \tag{2.87}$$

This is logical intuitively because if the plasma drift velocity is very large in relation to either the electron or ion mean velocity, then the electron's and the ion's velocities with respect to the grain are effectively just the drift velocity of the plasma. Solving equation 2.82 is very laborious. fortunately by resorting to experiment data, it is possible to simplify the situation. Studies have found flows on the order of $10^3 kms^1$ and 10^1 in the toroidal and poloidal directions respectively in the core plasma [37]. The toroidal measurements were collected from the JET, DIII-D and NSTX Tokamaks, and the poloidal data came from the JET, DIII-D and TFTR Tokamaks. We can gain a sense of the relevance of ion and electron flow respectively by comparing the data to ITER's benchmark operating temperature is around $13KeV$ with $T_e = T_i$. Calculating the electron and ion thermal speeds, $v_{te} = 1.33 \times 10^7 \sqrt{T_e}$, $v_{te} = 2.19 \times 10^5 \sqrt{T_d}$ and $v_{td} = 1.79 \times 10^5 \sqrt{T_d}$ (temperatures in KeV) implies that the toroidal normalised flow velocity is of order 1 (i.e. $mach \neq 1$ for the ions, but of order 10^{-2} for electrons. The poloidal flow is clearly insignificant. More pertinent to the problem in hand, Mach probe measurements of toroidal flows in the SOL of ASDEX Upgrade have also been made, finding flows on the order of mach 1 with respect to the ion sound speed, $C_{si} = \frac{k_B T_i}{m_i}$, for a D-D plasma (the only current Tokamak capable of operating with a D-T fuel mixture is JET and such experiments ceased in 1997 [13]) [25]. As a result it is clear that in the SOL off layer, and indeed in a Tokamak in general, we may ignore electron flows relative the electron thermal speed. In this case, SOML is simplified by replacing equation 2.81 with the original OML form, equation 2.44. Rewriting the floating condition then leads to equation 2.88 which has an analytic solution in terms of the Lambert W function, equation 2.89.

$$\exp\left(-\Phi_d^f\right) = \frac{1}{\sqrt{\mu\theta}}\left(\theta\eta_1\left(U_i\right) + \eta_2\left(U_i\Phi_d^f\right)\right) \tag{2.88}$$

$$\Phi_d^f = W\left[\frac{\sqrt{\mu\theta}}{\eta\left(U_i\right)}\exp\left(\frac{\theta\eta_1\left(U_i\right)}{\eta_2\left(U_i\right)}\right)\right] - \frac{\theta\eta_1\left(U_i\right)}{\eta_2\left(U_i\right)} \tag{2.89}$$

It can be shown that equation 2.89 reduces to the OML expression in the limit $U_i \to 0$ as was shown for the full SOML expression. This is confirmed by numerical solution to equation 2.89 which is plotted in figure 2.12 for various U_i. Note that when $U_i = (1+\gamma)$, this approximately corresponds to Mach 1 with respect to the ion sound speed. To see

this, observe that the ion sound speed in an arbitrary plasma is given by $c_s^2 = \frac{K_B T_e + \gamma K_B T_i}{m_i}$, but in a Tokamak where $T_i \approx T_e$, this reduces to $c_s^2 \approx \frac{(1+\gamma) k_B T_e}{m_i}$. All forms of the SOML

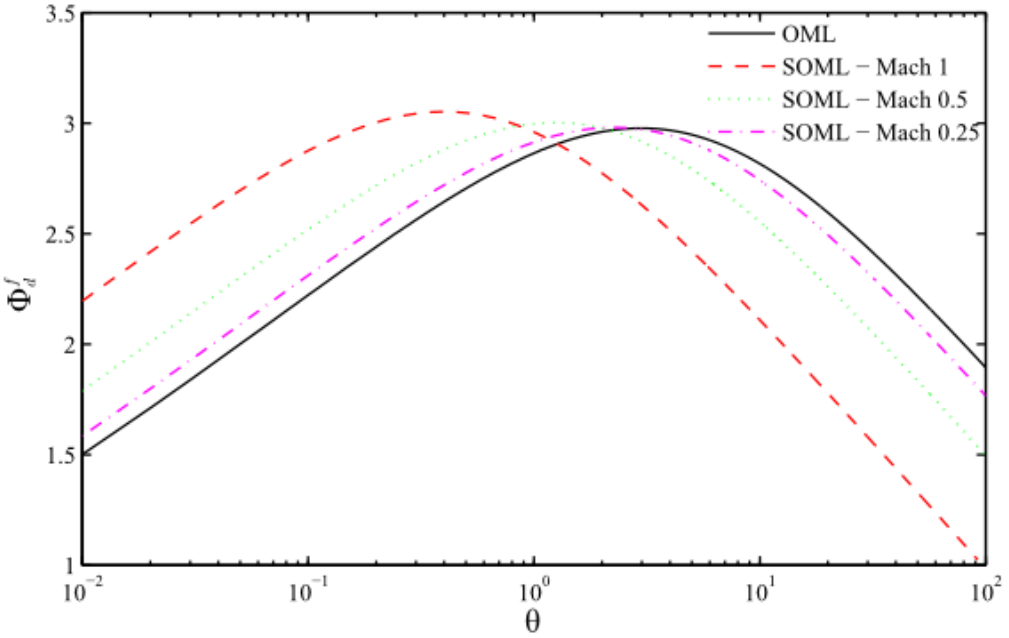

Fig. 2.12 The floating potential predicted by SOML neglecting electron flow for a 50-50 D+T plasma as a function of normalised ion temperature. The OML value is plotted for reference

floating equations have two severe shortcomings. The first is the problem shared from its parent theory OML that it fails to take into account the potential barriers arising from the formation of a sheath for the situation $A \gg 1$. In addition SOML is fundamentally invalalid from a theoretical perspective as strictly speaking the presence of a drifting Maxwellian distribution invalids the OML approach owing to the breaking of spherical symmetry and subsequently conservation of angular momentum. Recall it is precisely conservation of angular momentum which OML uses to place a limit on the ion current onto the grain. However, despite SOML's shortcoming, simulations run using the PIC code 'Sceptic' have provided good validation of SOML's floating current prediction [40]. As a result SOML is widely used, for instance in the DUSTT code [33]. Just as OML was extended to account for the potential barriers present in a large grain situation, so SOML can be extended in much the same way. The result is SMOML, where the 'M' stands for 'modified'.

2.2.6 Shifted Maxwellian Modified OML (SMOML)

SOML can be easily extended for large grains if electron flows are neglected. The electron current is again just the usual OML expression. However, the SMOML ion current is obtained by applying SOML to the sheath edge in the same way as in section 2.2.4. Therefore, the floating condition becomes:

$$\exp\left(-\Phi_d^f\right) = \frac{1}{\sqrt{\mu\theta}}\left[\theta\eta_1\left(U_i\right) + \frac{\eta_2\left(U_i\right)}{\theta}\left(\Phi_d^f - \frac{1}{2}\ln\left[\frac{2\pi}{\mu}\left(1+\gamma\theta\right)\right]\right)\right] \tag{2.90}$$

Just as before equation 2.90 may be written in the form $\Gamma\exp\left(\Gamma\right) = \kappa\left(\mu,\phi\right)$ and so once again it may be solved analytically using the Lambert W function, the result being given by equation 2.91.

$$\Phi_d^f = W\left[\frac{\sqrt{\mu\theta}}{\eta_2\left(U_i\right)}\exp\left(\Xi\left(\gamma,\theta,U_i\right)\right)\right] - \Xi\left(\gamma,\theta,U_i\right) \tag{2.91}$$

Where the function $\Xi\left(\gamma,\theta,U_i\right)$ is defined as:

$$\Xi\left(\gamma,\theta,U_i\right) = \frac{\theta\eta\left(U_1\right)}{\eta_2\left(U_i\right)} - \frac{1}{2}\ln\left[\frac{2\pi}{\mu}\left(1+\gamma\theta\right)\right] \tag{2.92}$$

From sections 2.2.4 and 2.2.5 it is readily apparent that equation 2.90 and by extension 2.91 reduce to the equation 2.56 as $U_i \to 0$. This can also be shown by the numerical solution as well whereby the SMOML value converges exactly onto the MOML value in that limit. Only plots for Mach 1 and 0.5 have been shown for clarity in figure 2.13 **??**

2.3 Summary Of Collection Theories

The ABR potential is a function of dust radius as it takes into account sheath effects by integrating the Poisson equation from the grain surface into the bulk. The resulting potential profile matches very well with the full OM theory in the limit $\theta < 1$ for large radii [15]. However, for small grains, the ABR theory departs from the full OM model. Since the OML potential is only a function of θ, it is difficult to compare ABR and OML since the latter does not reduce to the former in the appropriate limit. Indeed, the two theories are completely different, suggesting that the effects of ion angular momentum are significant. Thus it can be confirmed that assumption of radial motion for the ion current is not applicable to a Tokamak, since the ion angular momentum is certainly significant in the SOL where field flux surfaces are broken. It is shown in [15] that the Dëbye-Huckel provides a good estimate for the dust grain potential up to $A \sim 10^2$, supporting the use of OML in this regime. Exper-

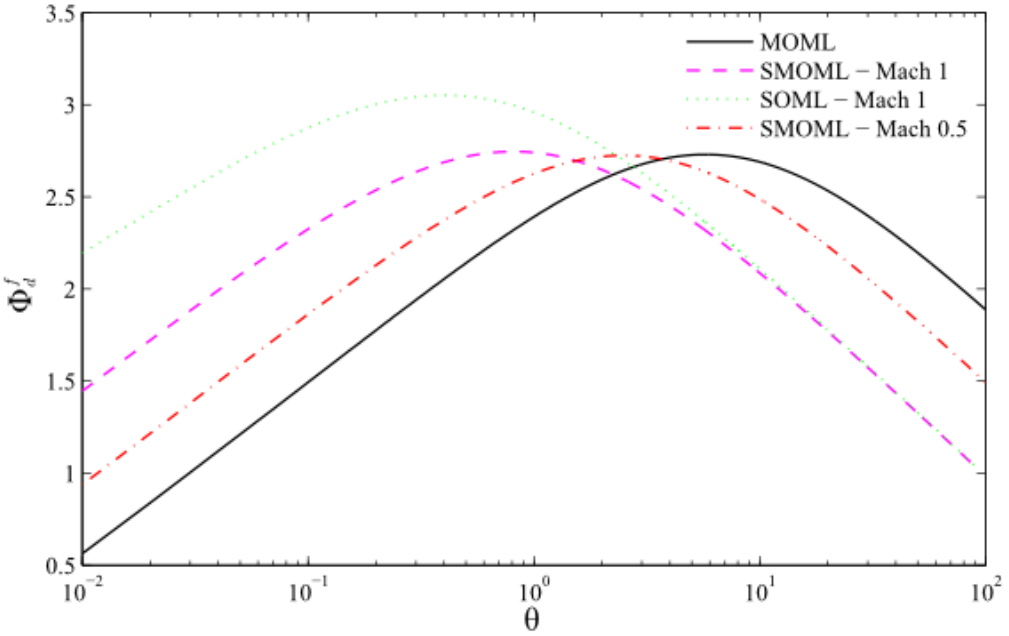

Fig. 2.13 The floating potential predicted by SMOML neglecting electron flow for a 50-50 D+T plasma as a function of normalised ion temperature for various values of normalised ion flow. The MOML value is plotted for reference.

iments show that almost all dust grains fall within this limit [29], and so together OML and MOML should provide a good estimate in the limit of low flow. The significance of flow for small and large grains is illustrated by figure 2.14. Flor $U_i \to 0$ it is confirmed that the flowless situation is the same as the non flowing situation. However, for $\theta < 1$, the flowing solution diverges from the non-flowing case by over 5% for speeds of around mach 1, that is $U_i \approx \frac{5}{3}$. For $\theta > 1$ the impact of flow becomes more and more sudden so that by $\theta \approx 4$, the shifted theories diverge rapidly from the stationary theories for $Ui \sim$ mach 1. In this regime, any charging model certainly needs to take account of flow.

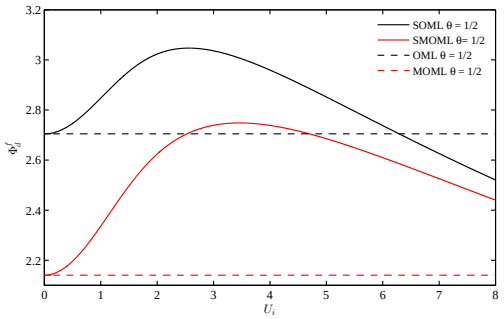

(a) $\theta = \frac{1}{2}$

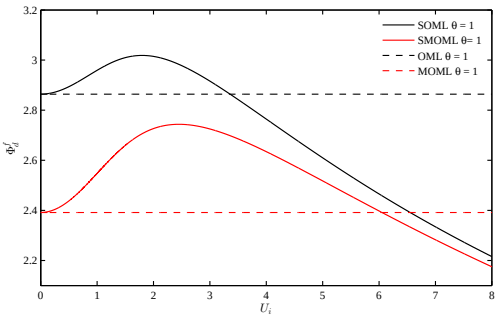

(b) $\theta = 1$

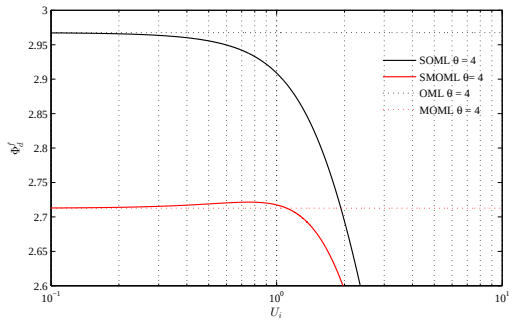

(c) $\theta = 4$ log scale

Fig. 2.14 Plots showing the variation of the floating potential for SOML and SMOML alongside the OML and MOML solution for $\theta = \frac{1}{2}$ and $\theta = 1$ with a D-T plasma assuming $\gamma = \frac{5}{3}$. Mach1 is approximately $2\frac{2}{3}$

Chapter 3

Positively Charged Grains and Dust Transport Codes

3.1 Charging By Emission

Conditions vary greatly in the SOL between the inboard and outboard regions. In the outboard side where the plasma surface interactions occur, typical parameters are $\lambda_{De} = 10^{-5}$, $T_e \sim 5ev$ and $n \sim 10^{17}$ [30]. The extreme conditions present in tokamak plasmas mean that other effects than just charge collection must be considered when computing the floating potential of a dust grain. The two electron emission mechanisms of interest in a Tokamak are 'Thermionic' and 'Secondary'. Under certain circumstances, the emitted flux can become larger than the ingoing flux in which case the dust grain can begin to charge positive [33]. In Tokamak plasmas, it is predicted that a few grains will gain a net positive charge. Considering any of the OML based models, in this situation the collected flux of electrons effectively become the ion expression and vice versa, and the collected currents could be computed as before. The following section gives expressions for the thermionic and secondary currents as used by the transport code DTOCKS, and outlines the DTOCKS charging model. Unfortunately time constraints have prevented the author from conducting a full theoretical review of the Thermionic and secondary Emission mechanisms as had been originally planned, so only the key formulae shall be provided here. The goal of this chapter is to outline the DTOCKS charging model and to see if its assumption of zero flow is important using the work on SOML.

3.1.1 Thermionic Emission

When a surface reaches a certain temperature, electrons or ions may be emitted from its surface by thermionic emission. The manifestation of thermionic emission exhibited by dust grains is derived from extensive work in space plasmas, see Whipple (1981) [39] for example. From such work, and from simulations run for tokamak plasmas, it is known that when the dust temperature $T_d \sim 3000K$, thermionic becomes the dominant charging mechanism [21]. The thermionically emitted electron current from a negative dust grain in a plasma is commonly given by the Richardson-Dushman formula, equation 3.1, where $A = 1.29173 \times 10^6 Am^{-2}K^{-2}$ is Richardson's constant [42], [39], [23], [26].

$$I_{th} = (P_b)\, 4\pi a^2 A T_d^2 \exp\left(-\frac{W_f}{k_B T_d}\right) \tag{3.1}$$

Where T_d is the temperature of the dust grain, and W_f is the work function of the dust grain material which is assumed to be constant.

3.1.2 Secondary Emission

An electron incident on a surface can either reflect or be absorbed. In the latter case and presuming the electron is sufficiently energetic, it can scatter with other electrons, stimulating the emission of other electrons. This process is known as 'Secondary Electron Emission' (SEE). SEE can also occur as a result of a flux of energetic ions. The SEE yield from a beam of monoenergetic electrons can be approximated by the equation 3.2, the Sternglass equation, where E is the energy of the beam [3]. Yields from SEE are typically in the $1-5ev$ range.

$$\frac{\Gamma_{sec}}{\Gamma_{max}} = (2.72)^2 \frac{E}{E_{max}} \exp\left(-2\sqrt{\frac{E}{E_{max}}}\right) \tag{3.2}$$

Where Γ_{sec} is the SEE yield from the surface for measured with an incident beam energy of E. Γ_{max} is the maximum SEE yield possible from that surface material in question, and E_{max} is the corresponding beam energy. Since the plasma electrons are a Maxwellian distribution and not a mono energetic beam, equation 3.2 may be integrated numerically to obtain $\Gamma(T_d)$ [4].

3.2 DTOCKS Charging Model

The papers relating to the following version of the DTOCKS charging mechanism date from between 2008 and 2012, references [23], [2] and [4]. A dust transport code consists of 3

elements:

1. Charging model
2. Transport model
3. Heating model

Only the charging model shall be reviewed although this is linked with the heating model since T_d is required to calculate the thermionic current.

DTOCKS uses standard flowless OML, modified to include thermionic and secondary emission. It utilizes the Richardson-Dushman and Sternglass Formulae respectively. Despite this, DTOCKS does not allow for grains with net positive charge. As in section 2.2.2, dust grains are assumed spherical with a spherical potential of the Dëbye-Huckel form. Magnetic effects are ignored despite the presence of fields of order $1T$ in the SOL. It has been estimated that including the magnetic field could result in a 30 % decrease in the value of the dust grain charge [33]. The flowless assumption is justified in [23] by the assumption that in the regime $v_d \sim$ mach 1, flows are more or less neglectable. The analysis presented in figure 2.14 lends support to this assumption in the low $theta$ limit as is assumed in DTOCKS [23]. However, it has become apparent that the assumption $T_i \approx T_e$, which is accurate in the core, is incorrect for the SOL. Recent measurements on the Tokamaks Tore Supra [24], ASDEX-Upgrade [19] and MAST [1] all indicate that $\theta > 1$, sometimes reaching as high as 16 [19] in the SOL. Tore Supra and ASDEX-Upgrade are both large aspect ratio Tokamaks similar to JET wheras MAST is a small aspect ratio 'spherical tokamak'. Since MAST is specifically used for the quality of its diagnostics, its mean value of $\theta = 4$ shall be taken as a guide. In this case, referring back to section 2.3, figure 2.14c suggests that SOML and OML will give significantly different answers for the dust grain charge and that flow is therefore important. It's interesting to note that the reason the approximation $T_i \approx T_e$ is relatively good for the core plasma is that as one moves in from the SOL towards the core, the collisionality increases, allowing the temperatures to equilibrate [6]. In order to account for electron emission, DTOCKS modifies the standard OML floating value. If the collected and emitted fluxes of electrons and ions are denoted as Γ_{em} and Γ_{col} respectively. Two scenarios are considered:

1. $Gamma_{col} \gg \Gamma_{em}$
2. $Gamma_{col} \approx \Gamma_{em}$ not considered see below.
3. $Gamma_{em} \gg \Gamma_{col}$

In the first case, the emitted electron current can be considered a perturbation to the original OML electron current. Then assuming that the OML potential maintains its Dëbye-Huckel form and there are no potential barriers preventing, the emitted electrons will all escape from the sheath structure and the floating condition may be written simply as $I_e \rightarrow I_{col} - I_{em} = I_{col}(1-\delta)$ where $\delta := \frac{I_{em}}{Icol}$. Applying the results of OML from section 2.2.2, the floating condition is $I_e + I_i = 0$, and equation 3.3 is obtained.

$$(1-\gamma)\exp\left(-\Phi_d^f\right) = \left(\frac{\theta}{\mu}\right)^{\frac{1}{2}}\left(1+\frac{\Phi_d^f}{\theta}\right) \tag{3.3}$$

The temperature in the coolest part of the SOL is around $5ev$, and so initially cold dust grains are expected to heat rapidly to beyond $T_d > 3000K$, the threshold when thermionic emission becomes dominant. Therefore the second limit is ignored and DTOCKS only considers the first and third situations [23]. In the latter scenario, PIC code simulations suggest that the grain potential is modified significantly by the presence of a potential barrier caused by the trapping of emitted electrons in the sheath [8], [9] as a result of the increased grain potential. The position of the potential barrier maximum shall be denoted b where $b > a$ so that the floating condition now has the form $I_e(a) + I_i(a) + I_{em}^{in}(a) - I_{em}^{out}(a) = 0$. Figure 3.1 gives a schematic of the form of the potential and illustrates the various emitted and collected currents. Since thermionic emission is dominant in this regime, the assumption that the emitted particles possess a Maxwellian distribution of temperature T_d suggests that the height of the potential barrier $\Delta\phi \approx \frac{k_B T_d}{e}$ [23]. Therefore, the original normalised OML potential is reduced by this quantity. Normalising as usual with respect to the electron temperature gives equation 3.4 [23]

$$\Phi_d^f = \Phi_{d,OML}^f - \frac{T_d}{T_e} \tag{3.4}$$

In order to compute the charge on the dust grain as a function of ϕ_d^f and a, it is necessary to estimate the capacitance, C_g, of the grain. Recall from section 2.1.1 that a probe in a plasma has associated with it a narrow space charge region of thickness $\sim \lambda_{De}$, the sheath. We must calculate the capacitance of the grain and sheath together. As usual spherical grains and therefore spherical sheaths are assumed so that the situation is just the textbook problem of the calculating capacitance between two concentric spheres. For a dust grain of radius a and a sheath of radius λ_{De} the solution is given by equation 3.5 [39]

$$C_g = 4\pi\varepsilon_0 a^2\left(\frac{1}{a}+\frac{1}{\lambda_{De}}\right) \tag{3.5}$$

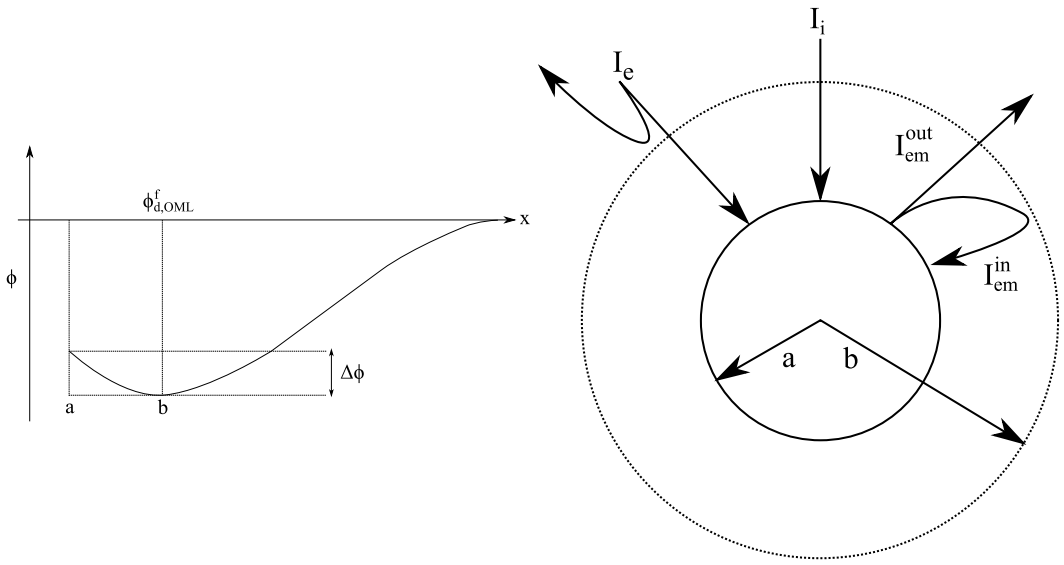

Fig. 3.1 Schematics showing (a) the form of the DTOCKS potential in the case where emission dominates the collection flux, and (b) the various collected (col) and emitted currents (em) to the grain [22]

Since DTOCKS uses straight OML which is only valid in the small grain limit $a \ll \lambda_{De}$, the capacitance is taken to be $C_g = 4\pi\varepsilon_0 a$. This is intuitively sensible since small dust grains don't possess a sheath. From the definition of the capacitance, we obtain equation 3.6, which provides an adequate estimate of the charge on a small dust grain Q_d.

$$Q_d = 4\pi\varepsilon_0 a\phi_d^f \tag{3.6}$$

DTOCKS is a pragmatic code, that is, at times precision is eschewed for computational expedience. For example, the assumption of a stationary Maxwellian is strictly incorrect, and the assumption that the height of the potential barrier in the preceding paragraph is $\approx \frac{k_B T_d}{e}$ was only heuristically justified. However, the work of chapter 2 has shown that flows are important in the regime of interest, $U_i \sim$ mach 1 and $\theta \approx 4$ (see figure **??**). In addition, figure 2.1 shows that there exist a significant fraction of dust grains for which $a \geq \lambda_{De}$ implying that a modified OML theory could be more applicable. It would be interesting to check the validity of SMOML for the regime of interest, as this model takes into account both the effects of flow and the sheath, albeit crudely. Certain Tokamaks e.g. LHD, which has the ability to run at steady state, has been found to have dust grains with average radius $10\mu m$, so in this case SMOML would readily apply. Another simplification is the assumption of spherical dust grains. An irregular shaped dust grain charging by collection, would obtain

angular momentum from the collected currents. The same goes for emitted currents. If the dust possessed angular momentum, it would not only lead to more more particle emission but would also affect the dust transport section of the code. Experiment shows that many dust grains are far from spherical [20]. [29], [14].

Chapter 4

Conclusions

4.1 Conclusion

Dust grain charging by collection has been reviewed in the cold ion, low flow, high flow, small radius and large radius limits. It has been shown that the inclusion of ion angular momentum is important for calculating the floating potential of a dust grain immersed in a tokamak plasma 2.2.1, 2.1.1 as are flows of order mach 1 2.3 and the presence of potential barriers associated with the formation of a sheath around larger dust grains 2.2.4. The OML theory has been presented in 4 guises:

1. OML: small grains without flow
2. SOML: small grains with flow
3. MOML: large grains without flow
4. SMOML: large grains with flow

Research has shown that one of DTOCKS' key assumptions, that $\theta \approx 1$ is incorrect, implying that flows should actually be accounted for. This suggests that DTOCKS may need to be modified to include SOML at least [24], [19], [1]. The assumption of small grains is also questionable since experiments on LHD have shown that in certain conditions, the average dust grain radius can be 10 times that of the Debye length [29]. In this case a combination charging model containing SOML and SMOML could perhaps be looked at. The ubiquity of OML theories in dust charging literature is primarily down to computational expediency for OML has many shortcomings. It was shown explicitly via the ABR solution, that the floating potential is an explicit function of grain radius. However, the basic OML solution is only a function of θ. This was also shown more explicitly in section 2.1.1, where it was

argued that the presence of large dust grains changes the structure of the plasma, introducing a quasi-neutral presheath and collisionless presheath. A full orbital motion theory does exist, but unfortunately such is its level of complexity that solutions are only available for a limited number of cases. Thus, OM is not much use for a dust transport code other than to act as a benchmark for a simplified charging model. Future work on the charging by collection problem could focus on attempting to constrain the trajectories of the collected particles. For instance, in tokamaks, particle transport is strongly supressed across field surfaces, but is uninhibited along them. Obtaining a constraint on particle motion could allow OML to be extended to contain explicit particle trajectories as with the ABR theory. The principle objection on theoretical grounds with the standard OML model is simply that it says nothing about these trajectories. In addition, an extension of this form could potentially open up the possibility of including magnetic effects, essential when the scenario of interest contains strong magnetic fields.

References

[1] Allan, S. (2013). Ion energy measurements on mast using a midplane rfea. *Journal of Nuclear Materials*, 438:192–195.

[2] Bacharis, M. (2009). *Theoretical Study of Dust in RF Discharges and Tokamak Plasmas*. PhD thesis, Imperial College London.

[3] Bacharis, M. et al. (2010). Dust in tokamaks: An overview of the physical model of the dust in tokamaks code. *Physics Of Plasmas*, 17:611–616.

[4] Bacharis, M. et al. (2012). Modelling of tungsten and beryllium dust in iter. *Plasma Phy. Control. Fusion*, 54.

[5] Bekris, N. (2005). Characterization of flakes generated in jet after dd and dt plasma operations. *Journal of Nuclear Materials*, 337-339:659–663.

[6] Brunner, D. et al. (2013). An assessment of ion temperature measurements in the boundary of the alcator c-mod tokamak and implications for ion fluid heat flux limiters. *Plasma Phys. Control. Fusion*, 55.

[7] Corless, R. M. et al. (1996). On the lambert w function. *Advances in Computational Mathematics*, 5.1:329–359.

[8] Delzanno, G. et al. (2005). Exact orbital motion theory of the shielding potential around an emitting, spherical body. *Physics of Plasmas*, 12:062102.

[9] G.L. Delzanno, G. L. and Rosenberg, M. (2004). Attractive potential around a thermionically emitting microparticle. *Phys. Rev. Lett.*, 92.

[10] Irvine, M. (2011). *Nuclear power : a very short introduction*. Oxford University Press.

[11] J. E. Allen, B. M. A. and de Angelis, U. (2003). On the orbital motion limited theory for a small body at floating potential in a maxwellian plasma. *J. Plasma Phys.*, 63:299–309.

[12] J. E. Allen, R. L. F. B. and Reynolds, P. (1957). The collection of positive ions by a probe immersed in a plasma. *Proc. Phys. Soc*, 70:297–304.

[13] Jacquinot, J. et al. (1999). Overview of iter physics deuteriumtritium experiments in JET. *Nuclear Fusion*, 39:235–253.

[14] Keiter, E. and Kushner, M. (1998). Plasma transport around dust agglomerates having complex shapes. *Journal of Applied Physics*, 83.

[15] Kennedy, R. V. (2001). *Potential Acquired by a Dust Particle Immersed in a Plasma*. PhD thesis, University of Oxford.

[16] Kennedy, R. V. and Allen, J. E. (2002). The floating potential of spherical probes and dust grains. part i: Radial motion theory. *J. Plasma Phys.*, 67:243–250.

[17] Kennedy, R. V. and Allen, J. E. (2003). The floating potential of spherical probes and dust grains. ii: Orbital motion theory. *J. Plasma Phys.*, 69:485–506.

[18] Kimura, H. and Mann, I. (1998). The electric charging of interstellar dust in the solar system and consequences for its dynamics. *THE ASTROPHYSICAL JOURNAL*, 499:454–462.

[19] Kocan, M. et al. (2011). Measurements of ion energies in the tokamak plasma boundary. *Journal of Nuclear Materials*, 415.

[20] Krasheninnikov, S. (2011). Dust in magnetic fusion devices. *Plasma Phys. Control. Fusion*, 53:083001.

[21] Krasheninnikov, S. I. et al. (2006). The 3d simulation of dust particle transport. *Contrib. Plasma Phys.*, 46:611–616.

[22] Martin, J. D. (2006). *Theory and Simulation of Dust in Tokamak Plasmas*. PhD thesis, Imperial College London.

[23] Martin, J. D. et al. (2008). Modelling dust transport in tokamaks. *EPL*, 83:347–371.

[24] M.Kocan et al. (2008). Edge ion-to-electron temperature ratio in the tore supra tokamak. *Plasma Phys. Control. Fusion*, 50.

[25] Muller, H. et al. (2007). Deuterium plasma flow in the scrape-off layer of asdex upgrade. *Journal of Nuclear Materials*, 363-365:605–610.

[26] Pigarov, A. et al. (2005). Dust particle transport in tokamak edge plasmas. *Physics of Plasmas*, 12:122508.

[27] Riemann, K. (1991). The bohm criterion and sheath formation. *J. Phys. D: Appl. Phys*, 24:493–518.

[28] S. P. Hirshman, D. J. S. (1981). Neoclassical transport of impurities in tokamak plasmas. *Nuclear Fusion*, 21:1079–1201.

[29] Sharpe, J. et al. (2003). Characterization of dust collected from asdex-upgrade and lhd. *Journal of Nuclear Materials*, 313-316:455–459.

[30] Sharpe, J. P. et al. (2002). A review of dust in fusion devices: Implications for safety and operational performance. *Fusion Engineering and Design*, 63-64:153–163.

[31] Shimomura, Y. et al. (1999). Iter overview. *Nuclear Fusion*, 39:1295–1308.

[32] Shukla, P. K. and Mamun, A. A. (2001). *Introduction to Dusty Plasmas*. Institute of Physics Publishing.

[33] Smirnov, R. D. et al. (2007). Modelling of dynamics and transport of carbon dust particles in tokamaks. *Plasma Phys. Control. Fusion*, 49:347–371.

[34] Stacey, W. M. (2005). *Fusion plasma physics*. Wiley - VCH.

[35] Stangeby, P. (2000). *The Plasma Boundary of Magnetic Fusion Devices*. Institute of Physics Publishing.

[36] Stangeby, P. C. and McCracken, G. M. (1990). Reviww paper: Plasma boundary phenomena in tokamaks. *Nuclear Fusion*, 30.

[37] Thyagaraja, A. and McClements, K. G. (2006). Toroidal and poloidal flows in single-fluid and two-fluid tokamak equilibria. *PHYSICS OF PLASMAS*, 13.

[38] Wesson, J. (1987). *Tokamaks*. Oxford University Press.

[39] Whipple, E. (1981). Potentials of surfaces in space. *Rep. Prog. Phys.*, 44:1197–1243.

[40] Willis, C. T. N. et al. (2012). The floating potential of large dust grains in a collisionless, flowing plasma. *Phys. Rev.*, 85.

[41] Wilson, G. R. (1995). Development of non-maxwellian velocity distributions as a consequence of nonlocal coulomb collisions. *Cross-Scale Coupling in Space Plasmas*, pages 47–60.

[42] Wu, H.-C. and Xie, B.-S. (2005). Effect of thermionic emission current on charge of grains in plasma. *Physics of Plasmas*, 12:064503.

Appendix A

The ABR Solution

Extensively documented MATLAB code is provided for obtaining the ABR floating potential value as a function of grain radius.

```
%SOLVE the ABR Poisson equation to calculate how the potential varies from
%the plasma solution to the grain. The ABR Poisson equation,
%d2vdx2 = j*v^(-1/2)/x^(2) - exp(-v) - 2*dvdx/x is integrated from a point
in quasi-neutral plasma, initial_x, inwards to an arbitrary radius, end_point.
%The boundary values are denoted 'initial_dvdx' and 'initial_v'.

function ABRsolution
format long
gam=1e3; %Gam is an arbitrarily large adjustable parameter (same for each
%set of curves in a given calculation. The calculation was found to be
insensitive to Gam>1e3).

The Poisson equation is integrated from initial_x to end_point. However,
it has been found that 'ode45' is unstable when integrating 'backwards' so
%we make a change of variables, x = initial_x - xnew and integrate forwards
from xnew = 0 to xnew = initial_x - 0.01.
%The function 'rhs(xnew,v)' contains the Poisson equation broken up into
%a system of two first order differential equations with the change of
%variables above implemented.

end_point=1e-2;

for j = 5:25:100
    initial_v=double(bdryV(j,gam)); %Function included for completed below
    initial_x=double(bdryX(j,initial_v)); %--------------------------------
    initial_dvdx=double(bdrydV(initial_x,initial_v,j)); %-----------------
```

```
    xnew=0:0.0001:initial_x- end_point; %Integration range
    options=odeset('Refine',12);
    [xnew,v]=ode45( @rhs, xnew, [initial_v initial_dvdx],options);

%Convert back to the original variables to produce the potential curves
for selected J.
    x=initial_x-xnew;
    plot(x,v(:,1));
    hold on


%Below the grid for the interpolation used to find the point where the ABR
%floating condition crosses with the potential v(x)
%fineness = step size for x_fine. Set a large ending value in x_fine for
%large values of j otherwise vector will be too small to take the floating
%point values
    fineness=1e-2;
    x_fine=end_point:fineness:1e4;
    crosspoint(x,v(:,1),j,x_fine);
%convert the indes number 'float_point' in x_fine to the gird coordinate in
%x
    float_point= end_point+ fineness*crosspoint(x,v(:,1),j,x_fine);
%convert float point to index number in x

%'spline(x,v(:,1)) performs a spline interpolation on v(:,1) to estimate the
potential value corresponding to the coordinate 'float_point'.

    float_pot=spline(x,v(:,1),float_point);
    plot(float_point,float_pot);
    hold on

%Finally produce the floating potential graph. The function 'ABRfloat(j,v_f)'
%inputs matching values of j to potential values, outputting values for
%the matching dust grain radius. The intersection between the two
%curves on the resultant plot gives the floating potential at A.
    plot(x,ABRfloat(j,x))
    hold on
end

xlabel('\(X\)','Interpreter','LaTex','FontSize',11)
ylabel('\(\Phi\)','Interpreter','LaTex','FontSize',11)

    function dvdx=rhs(xnew,v)
        dvdx_1 = v(2);
```

```
        dvdx_2 = j*v(1)^(-1/2)*(initial_x-xnew).^(-2) - exp(-v(1)) + 2*(initial_x -xn
        dvdx = [dvdx_1; dvdx_2];
    end

end
```

Listed below for completeness are the short functions bdryV(j,gam), bdryX(j,initial_v), bdrydV(initial_x,initial_v,j), crosspoint(x,v(:,1),j,x_fine) and ABRfloat(j,x) should the reader wish investigate the ABR solution further. It is noted that the author produced the calculations on a home laptop.

```
function v_b = bdryV(j,gam)
syms z
v_b=vpasolve(j-gam*(4.*z^(1.5)*(2*z-3)*(2*z+1)/((2*z-1)^(3))) == 0, z,[0,1]);
end

function x_b = bdryX(j,v_b)
x_b = j^(1/2)*exp(v_b/2)/(v_b^0.25);
end

function dv = bdrydV(initial_x,initial_v,j)
dv=2*initial_x*initial_v^1.5*exp(-initial_v)/(j*(initial_v-0.5));
end


function x_point = crosspoint(xcoarse,v,j,x_fine)

%function to calculate the points at which the analytic floating condition
%function crosses with the potentials calculated in 'ABRsolution'.
%Uses spline interpolation to find where the difference between the
%floating value and integrated value changes sign. The first point is taken
%as the crosspoint and thus the floating point at the corresponding radius.

differences=ABRfloat(j,x_fine)-spline(xcoarse,v,x_fine);

differences(differences>0)=1;
differences(differences<0)=0;

%x_point is the index in x_fine corresponding to the floating potential at
%that particular of j. Note, the problem is not overspecified since each
%value of j corresponds to a particular radius.
x_point=find(diff(differences)~=0);
end
```

```
33
34 function v_f = ABRfloat(j,A)
35 %calculate the allowed floating potential values for a given J
36 mu=1836*2.5;
37 v_f = 0.5.*log(A.^4*mu./(4*pi*j.^2));
38 end
```